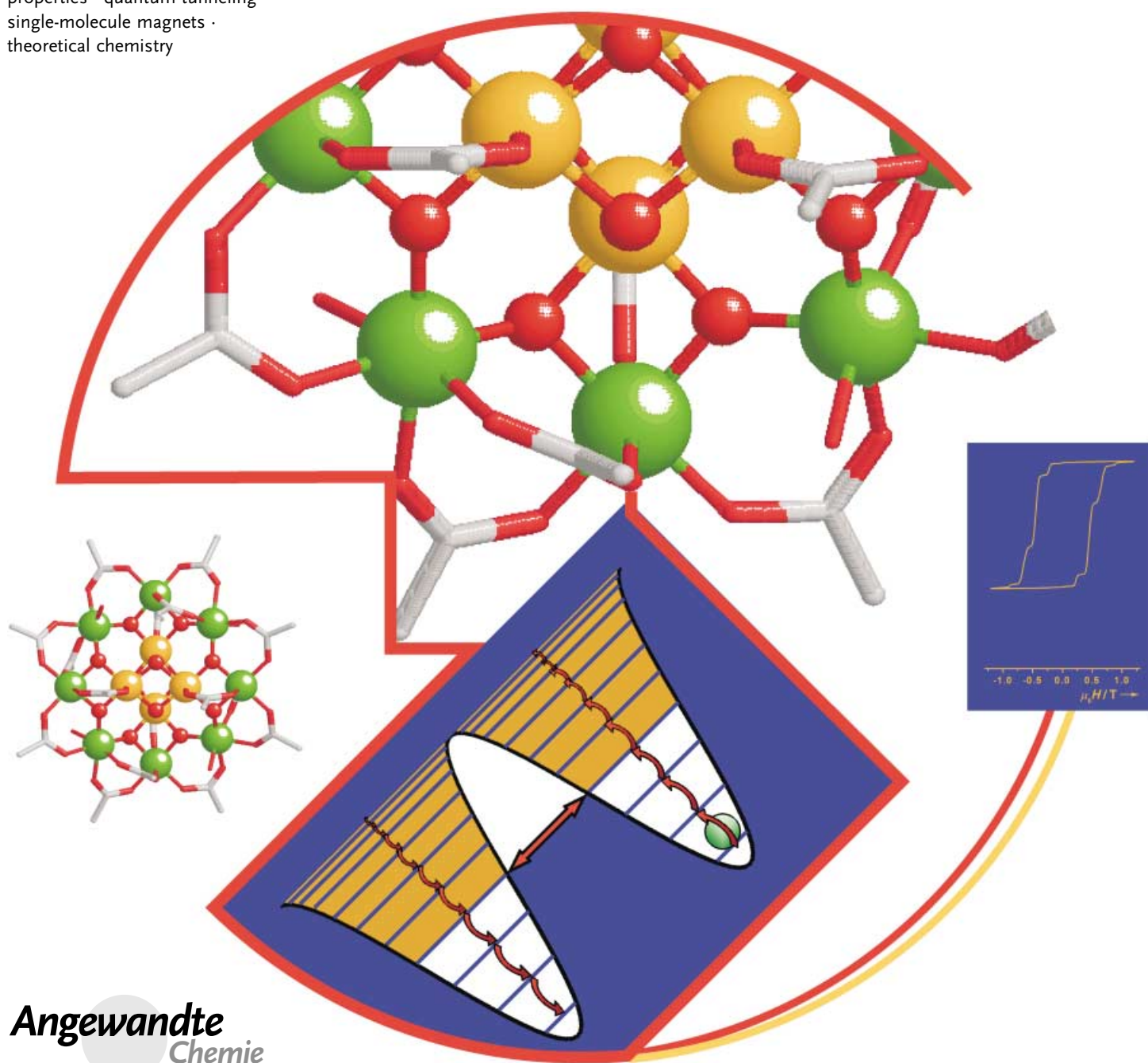# Quantum Tunneling of Magnetization and Related Phenomena in Molecular Materials

Dante Gatteschi and Roberta Sessoli*

Molecules comprising a large number of coupled paramagnetic centers are attracting much interest because they may show properties which are intermediate between those of simple paramagnets and classical bulk magnets and provide unambiguous evidence of quantum size effects in magnets. To date, two cluster families, usually referred to as Mn12 and Fe8, have been used to test theories. However, it is reasonable to predict that other classes of molecules will be discovered which have similar or superior properties. To do this it is necessary that synthetic chemists have a good understanding of the correlation between the structure and properties of the molecules, for this it is necessary that concepts such as quantum tunneling, quantum coherence, quantum oscillations are understood. The goal of this article is to review the fundamental concepts needed to understand quantum size effects in molecular magnets and to critically report what has been done in the field to date.

From the Contents

1. Introduction

The fields in which chemistry may have a fundamental role are increasing in number, and it is becoming more and more difficult (though stimulating) for synthetic chemists to cope with requests of new compounds with highly sophisticated properties. The movement from simplicity to complexity in molecular chemistry is one which cannot be stopped, and supramolecular chemistry is just one clear example of that.[1]

The last few years have seen the opening of many new research fields in which molecular materials have been forced, through chemical ingenuity, to acquire properties which are associated with classic inorganic materials. Perhaps the most convincing evidence for this has been the development of purely organic materials, which behave as conductors and superconductors. In addition, organic materials, because of their photorefractive and nonlinear-optical properties, are now even used to make lasers.[2,3]

Magnetism is certainly one of the fundamental properties of matter, inextricably associated with electrical properties, and molecular magnetic materials have recently become a hot topic, thanks to the efforts of many research groups. In particular the role of a pioneer of the field, the late Olivier Kahn, must be recognized.[4,5] One of the main difficulties in developing molecule-based magnets is that bulk magnetism is intrinsically a three-dimensional (3D) property in that only if a 3D lattice of interacting magnetic centers is assembled may the material show spontaneous magnetization below a critical temperature. The problem with molecular materials is that the design of genuine 3D connected lattices is not obvious, because the intrinsic low symmetry of the individual molecules tends to favor 1D or 2D arrangements. Here the difference between molecular magnets and conductors is striking, because for conductors exciting properties can be found even if 1D arrangements of individual molecules are obtained in the solid state. However, this has not scared the synthetic chemists and genuine room-temperature molecule-based magnets are now available. The field has been well reviewed in recent years and the interested reader is addressed to the cited literature.[6–9]

The difficulties in forming 3D magnets with molecular materials have been turned into advantages when it was realized that oligonuclear compounds, comprising a large, but finite, number of magnetic centers may have unique magnetic properties which have made them almost ideal systems for observing quantum size effects in magnets.[10–14] The magnetic centers can be transition-metal or rare-earth ions, or even organic radicals. The observation of quantum phenomena in mesoscopic matter[15] provides, in principle, confirmation to the so-called Copenhagen interpretation, which assumes that there is a continuous transition from the field of small objects, where quantum mechanics is required, to macroscopic objects, where classical physics operates well. Materials the properties of which are intermediate between classical and quantum nature, or where there is coexistence of the two, may be used for completely new types of devices. A particularly interesting field is that of quantum computing,[16] where information can be handled taking advantage of quantum

[*] Prof. Dr. R. Sessoli, Prof. Dr. D. Gatteschi
Department of Chemistry
University of Florence, UdR INSTM
Polo scientifico universitario, via della Lastruccia 3
50019 Sesto Fiorentino (Italy)
Fax: (+ 39)-055-4573372
E-mail: roberta.sessoli@unifi.it

effects. Research is very active in this field, on systems ranging from the NMR of molecules[16] to Josephson junctions.[17] In principle it is also possible to consider magnets in this perspective,[18] as these have long been suggested to give rise to quantum effects in mesoscopic objects.

At the beginning of the 1990s it was discovered[19, 20] that a molecule, comprising 12 manganese ions, and characterized by a ground state with $S = 10$, $[Mn_{12}O_{12}(CH_3COO)_{16}(H_2O)_4]$ (Mn12ac),[21] shows slow relaxation of the magnetization at low temperature (of the order of months at 2 K). Under these conditions a single molecule becomes like a tiny magnet, in the sense that if magnetized by an applied field it retains the magnetization for days. In fact it gives rise to magnetic hysteresis, which is one condition for storing information in a particle. Under this respect therefore Mn12ac behaves like a classical magnet. However, it is still small enough to also show large quantum effects. In fact Mn12ac, and other molecules which have since been investigated, provide the best examples to date of the observation of quantum effects, such as the tunneling of the magnetization, in magnets. These molecules are now often called "single-molecule magnets"[22] (SMMs). The name itself is not correct, because to have a magnet it is necessary to have an infinite number of coupled centers, but is evocative, and in our opinion it can be used provided the above *caveat* is taken into consideration.[11,23]

Herein we wish to review the current state of the art in the field of SMMs, and in particular highlight the numerous and complex quantum phenomena that can be observed in this new class of molecular materials. The field of SMMs is an interdisciplinary one, where many papers are published in physics and chemistry journals. To design new classes of molecules with enhanced SMM properties the chemical community must be aware of the development of the physical treatment of SMMs. Thus, the reader must be prepared to digest a little quantum mechanics; we will try to provide the basic introduction, in as brief and clear a form as possible.

2. Quantum Tunneling and Quantum Coherence

It all started with Schrödinger's cat: the poor animal was the first macroscopic object for which quantum phenomena were envisaged as possible, and the agonizing result was that it remained uncertain whether it was alive or dead. More seriously, macroscopic objects may be stable in two different states, but they can have only one state at a time. If we consider a ball in a container characterized by two wells (Figure 1 a), it may be either in the left or in the right well, but once a choice is made it is clear that its state is described for instance by the statement: the ball is in the right well. It can change its state, by overcoming the barrier Δ_B separating the two wells, and then roll down into the left well. A quantum object on the other hand has also a wave nature, and if the wavefunction of the left-hand particle extends over to the right-hand well, and vice versa, the state of the particle must be described by a superposition of the two states. Since the wavefunction of the left well extends to the right wall with a nonzero value, the probability of observing the left ball in the right well is different from zero: therefore the ball can be both in the right- and in the left-hand well. It is as if the particle could pass from left to right without climbing the barrier, but tunneling; the effect is in fact called quantum tunneling, and is one of the most typical manifestations of quantum mechanics. Some typical examples are observed in small molecules, such as ammonia, where the inversion of the NH_3 bonds occurs exactly with this mechanism. Hydrogen tunneling has been observed in enzyme catalysis,[24] and recently also in a hydrogen-bond network containing calyx[4]arene molecules.[25] There is no theoretical limitation that in principle forbids observing quantum effects in larger particles, although it is known that the tunneling probability scales exponentially with the barrier height and the particle mass. Therefore it is expected to be most observable in small particles and at low temperatures.

The actual possibility of observing tunneling depends on the extent of the interaction of the two wavefunctions. In fact, if the two wavefunctions overlap there must be an interaction between them which splits the two degenerate levels in the
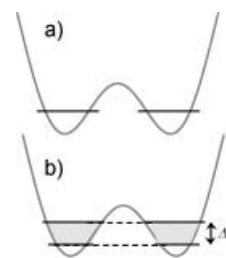

Figure 1. Tunneling in a double well system. a) Noninteracting states; b) interacting states giving rise to tunnel splitting Δ_T.

Dante Gatteschi was born in Florence in 1945. He graduated in Chemistry at the University of Florence in 1969. He became the assistant of Professor Sacconi and in 1980 he became Professor of Chemistry in the same University. His research interests lie in the electronic structure of transition-metal complexes, in EPR spectroscopy, and in the last few years in molecular magnetism. In 1979 he was awarded by the Italian Chemical society the Nasini prize and in 1992 the Magnetic Resonance Award. In 2000 he was awarded the Bruker Prize for his contributions to EPR spectroscopy and in 2002 he shared with Roberta Sessoli and three other colleagues the Agilent Europhysics Prize.

Roberta Sessoli, born in 1963, graduated in chemistry at the University of Florence in 1987 and received her PhD in 1992 for work on molecular magnetism. She is now Associate Professor at the Faculty of Pharmacy at the University of Florence. Her current interests are the study of slow dynamics of magnetization in one-dimensional molecular compounds. For her work on the static and dynamic magnetic properties of high spin clusters she was recently awarded the 2002 Agilent Technologies Europhysics Prize that she shares with Dante Gatteschi and three other colleagues.

270

Angew. Chem. Int. Ed. **2003**, *42*, 268–297

left and right well, giving rise to a so-called tunnel splitting, Δ_T (Figure 1 b). One of the two coupled levels is of lower energy than the degenerate levels, while the other is of higher energy, exactly like a pair of bonding–antibonding levels in elementary MO theory. The possibility of tunneling is related to the relative energies of the tunnel splitting and of the barrier. The smaller the ratio between the two the smaller the possibility of observing tunneling.

So far we have considered the system of the particle in the two wells as completely separated from the environment. This is clearly an approximation, because the interaction with the environment can be minimized, but not completely eliminated. If the particle is localized in a metastable state (Figure 2), it can tunnel out of the metastable state. No energy is involved if the particle is isolated from the environment, whereas coupling to the environment means that the particle loses energy with the tunneling (as shown by the arrows in Figure 2). The interactions with the environment will tend to localize the particles, because the interactions will make one well more "attractive" than the other (that is, reduce the energy of one of the wells). In the case of strong coupling with the environment, which means that this interaction is much larger than the tunnel splitting, the particle will stay localized in one of the two wells, and will not tunnel. For intermediate coupling the particle can tunnel, but jumping incoherently from one well to the other. This means that one particle will tunnel, and localize for some time in the other well, and then tunnel again, but in an irregular way. The third case is that of weak coupling when the tunnel splitting is large compared to the interaction with the environment, and the particle oscillates coherently between the two minima. The conditions for observing coherent tunneling are severe. Evidence for coherent tunneling is the observation of energy absorption at a frequency corresponding to the tunnel splitting. In the above experiment of calyx[4]arene a peak was observed in the proton-spin lattice-relaxation rate at a field corresponding to the tunneling frequency of 35 MHz.[25]

In the above discussion we did not take into account the origin of the interaction between the two wavefunctions. It is apparent that in the description we have made some implicit assumptions: 1) that an unperturbed Hamiltonian, $\mathcal{H}_0$, gives the initial description with the two equivalent wells, 2) a perturbation Hamiltonian, $\mathcal{H}_1$, is added which couples the two separate states and removes the degeneration, 3) a Hamiltonian describing the interaction with the environment, $\mathcal{H}_2$, is needed [Eq. (1)].

$$\mathcal{H} = \mathcal{H}_0 + \mathcal{H}_1 + \mathcal{H}_2 \tag{1}$$

The actual form of the three relevant Hamiltonians will depend on the nature of the system taken into consideration. In this article we will be focussing on magnetic systems, therefore we will limit the description to such systems.

Figure 2. Tunneling from a metastable state.

3. Magnetic Relaxation in Systems with Large Spin

Let us consider a system with a well defined ground spin state, characterized by a large value of S (for example Mn12ac with $S = 10$). The unperturbed Hamiltonian includes the effect of an external magnetic field parallel to the unique axis of the cluster and of its axial splitting as a result of crystal-field effects. At this level of approximation only the second-order crystal-field effects will be included. Therefore, for the discussion we wish to develop,[26] the $\mathcal{H}_0$ Hamiltonian can be written as Equation (2) where D is a negative constant for the system of interest and H_z is the magnetic field strength in the z direction. D is one of the parameters of the so-called Zero Field Splitting (ZFS) because it removes the degeneracy of the S multiplet.

$$\mathcal{H}_0 = D\,[S_z^2 - S(S+1)/3] + g\,\mu_B\,H_z\,S_z \tag{2}$$

The energies of the spin levels corresponding to $\mathcal{H}_0$ are in fact easy to calculate as given by Equation (3), where $-S \leq M_S \leq S$.

$$E(M_S) = D\,(M_S^2 - 110/3) + g\,\mu_B\,M_S\,H_z \tag{3}$$

The energy levels can be plotted as shown in Figure 3 a. When no external field is applied all the levels are degenerate pairs, except $M_S = 0$. Since D is negative the $M_S = \pm S$ levels will lie lowest. In Figure 3 the states with positive M_S are plotted in one potential well, and those with negative M_S in the other. This formalism is an extension of that commonly used for superparamagnets (see below).[27] A system like this is characterized by magnetic anisotropy along the "easy axis", which means that the magnetization is preferentially oriented parallel to the z axis.
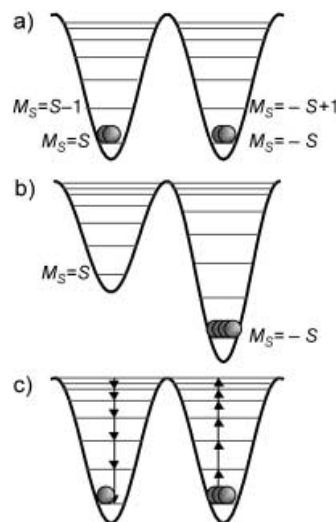
Figure 3. Energy levels for a spin state S with easy axis magnetic anisotropy. The $+M$ levels are localized in the left well and the $-M$ levels in the right well. a) In zero field the two wells are equally populated; b) the application of a magnetic field selectively populates the right well; c) after removing the field the return to equilibrium occurs through a series of steps.

When a field is applied parallel to the z axis the levels characterized by a positive M_S correspond to a projection of the magnetization antiparallel to the field, while those with negative M_S correspond to magnetization parallel to the applied external field (Figure 3 b). The separation in zero field between the $|M_S|$ and $|M_S-1|$ levels is given by $(2|M_S|-1)|D|$. The system can be prepared in a magnetized state by applying a magnetic field parallel to the z axis. If T is low and H_z large the $M_S = -10$ state will be the only one populated and the magnetization reaches the saturation value. When the field is removed the system must go back to thermal equilibrium ("relaxation"; Figure 3 c). This means that at the equilibrium half of the molecules must be in the $M_S = -10$ and half in the $M_S = +10$ state, with no resulting magnetization. The relaxation (the return to the equilibrium) can be monitored by measuring the magnetization as a function of time ($M(t)$). For a simple system this occurs with an exponential decay [Eq. (4); τ = relaxation time].

$$M_z(t) = M_z(t=0)\exp(-t/\tau) \tag{4}$$

The relaxation process is made possible by the coupling of the spin system to the environment. An important source of coupling is the spin-phonon interaction, which originates from the perturbation of the crystal field induced by lattice vibrations. The spin-phonon Hamiltonian contains terms quadratic in the spin operators.[28,29] Therefore, the allowed transitions are from a state $|M_S\rangle$ to $|M_S\pm 1\rangle$ and $|M_S\pm 2\rangle$. However, for the sake of simplicity we can consider only the terms that connect $|M_S\rangle$ to $|M_S\pm 1\rangle$. In particular, by coupling to vibrations (phonon coupling) a given molecule can change its state from $M_S = -10$ to $M_S = -9$ by absorbing one quantum which corresponds to the difference in energy $E(-9)-E(-10)$. The process can be repeated to go to $M_S = -8$, then $M_S = -7$, until $M_S = 0$ is reached. From this state the spin can lose its energy by emitting phonons, that is, exciting vibrational modes of the lattice, to reach the $M_S = +10$ state, or to return to the $M_S = -10$ state. The theoretical expression for the relaxation rate requires the calculation of the transition probability, γ_p^q, from one state, with $M_S = p$, to the other, with $M_S = q$, mediated by spin-phonon coupling V_{pq}. After some approximation the transition probability can be expressed as Equation (5) (for $E(q) > E(p)$) and Equation (6) (for $E(q) < E(p)$).[29]

$$\gamma_p^q \propto |V_{pq}|^2[(E(q)-E(p))]^3[1-\exp((E(q)-E(p))/kT)]^{-1} \tag{5}$$

$$\gamma_p^q \propto |V_{pq}|^2[(E(p)-E(q))]^3[\exp((E(p)-E(q))/kT)-1]^{-1} \tag{6}$$

The transition probabilities in Equation (5), which correspond to increasing the energy, become extremely small at low temperature. The probability per unit time, to go to the top of the barrier, is proportional to the product of the exponentials $\exp((E(q)-E(p))/kT)$, of the individual ladder steps to go from $M_S = -10$ to $M_S = 0$, which in a weak field corresponds to $\exp((E(0)-E(-10))/kT)$. The quantity $E(0)-E(S) = \Delta E$ corresponds therefore to a barrier to be overcome in the relaxation process. By writing a set of master equations, where the variation per unit of time of the population M is related to the transition probabilities, Villain et al.[29] have obtained the Equations (7a,b) for the relaxation time τ in the limit $kT \ll \Delta E$ and a weak magnetic field, where ρ is the speed of sound in the material and c is the speed of light in a vacuum.

$$\tau = \tau_0 \exp(\Delta E/kT) \tag{7a}$$

$$\tau_0 = \frac{2\pi}{3}\frac{\hbar^2\rho c^5}{|V_{10}|}\left[\frac{S^2}{\Delta E}\right]^3 \tag{7b}$$

The spin-phonon matrix element in τ_0 is V_{10} because the last step in climbing the barrier is the slowest one, thus determining the rate of the entire process. The relaxation rate therefore follows the Arrhenius law, where the barrier ΔE is the difference in energy between the $M_S = \pm S$ states and the highest one(s), that is $-DS^2$ for integer spin and $-D(S^2-\frac{1}{4})$ for half-integer spin values.

This behavior is the same as that observed for superparamagnets (classical magnetic particles). These are small particles of bulk magnets, in which the magnetic anisotropy is comparable to the thermal energy.[27] Actually they can be considered as systems with extremely high S (of the order of 10^3 or larger). The main difference to our $S = 10$ system is that the energy levels within the potential wells of the superparamagnets give rise to a quasicontinuum. Another important consequence of the theoretical treatment of the pre-exponential factor τ_0 is that it is expected to be proportional to $[S^2/\Delta E]^3$ and therefore $\tau_0 \propto |D|^{-3}$. However, for a given ΔE barrier the higher the value of the spin S the longer the relaxation time. Therefore, rather expectedly, the strategy to observe a long relaxation time is that of synthesizing clusters with large spin S and large zero-field splitting.

4. Spin Tunneling: Zero-Field Case

At low temperature only the degenerate $M_S = \pm 10$ levels will be populated, but, as long as the Hamiltonian $\mathscr{H}_0$ [Eq. (2)] is valid the two states are orthogonal to each other, and there is no possibility of tunneling. In principle, since the two states are degenerate, every linear combination will be an eigenfunction of the system. But to observe tunneling the two functions must be admixed by some suitable perturbation. Therefore, if we want to observe tunneling we must introduce the perturbation Hamiltonian $\mathscr{H}_1$ that allows the mixing of the two states. The tunneling process involving otherwise degenerate levels is named resonant tunneling.[30–32]

From the physical point of view it is possible to think of a distortion which removes the axial symmetry that we have assumed for $\mathscr{H}_0$. This situation corresponds to the introduction of an anisotropy in the xy plane, or, as it is often called, a transverse anisotropy. A convenient form for the $\mathscr{H}_1$ Hamiltonian is Equation (8) where E is a parameter, which, without loss of generality,[33] is limited to be $0 \le |E/D| \le \frac{1}{3}$.

$$\mathscr{H}_1 = E(S_x^2 - S_y^2) \tag{8}$$

272

Angew. Chem. Int. Ed. **2003**, *42*, 268–297

In the case considered so far, if E is positive the spins in the xy plane will try to avoid the x axis, which is called the hard axis, while y is the intermediate axis. The Hamiltonian $\mathscr{H}_1$ does not commute with $\mathscr{H}_0$, therefore the eigenstates of the full Hamiltonian $\mathscr{H} = \mathscr{H}_0 + \mathscr{H}_1$ are an admixture of $|M_S\rangle$ states, also with different sign of M. The wavefunction is therefore partially delocalized on both wells and this may give rise to tunneling. However, Equation (8) directly couples states differing in M_S by ± 2. Therefore in first-order perturbation theory $M_S = +10$ admixes with $M_S = +8$, and $M_S = -10$ with $M_S = -8$, but no admixture of $M_S = +10$ and $M_S = -10$ is possible at this level of approximation. Of course $M_S = +8$ is coupled to $M_S = +6$, and this to $M_S = +4$, etc. Therefore an admixture is possible for the $M_S = \pm 10$ states, but only at the tenth order in perturbation theory and the tunnel splitting Δ_T of the $M_S = \pm 10$ levels will be extremely low. Matters are different for the higher energy levels where for instance the $M_S = \pm 2$ levels are split in second-order perturbation theory.

The energy levels appropriate to the Hamiltonian, which include the transverse anisotropy term [Eq. (8)], can be easily calculated by diagonalizing the 21×21 matrix of the $2S + 1$ states. The results are plotted in Figure 4, which shows the energy levels in the presence of an applied magnetic field parallel to the z axis, the so-called easy axis, where the largest magnetization is observed. It is apparent that for small values of E/D the highest energy levels begin to split even in zero field, while the lowest-lying levels remain essentially degenerate, which confirms the above qualitative discussion. For the lowest-lying levels a perturbation description is still appropriate, while for the highest energy levels it loses significance. However, since we are interested at the behavior at low temperature, where only the lowest-lying levels will be populated, the perturbation approach remains valid.

The $M_S = \pm 1$ levels (remember that this notation is rigorously meaningful only for $E/D = 0$ because with $E \neq 0$ states with different M_S will be admixed) show the largest splitting (insert in Figure 4), followed by the $M_S = \pm 2$ levels, while all the others remain essentially not split. On increasing the transverse anisotropy further, matters become more complex on the high part of the graph, because of the extensive mixing of the levels. An interesting feature is that new quasidegeneracies are established, which show up clearly at the $E/D = 1/3$ limit. The levels become symmetrically spaced, with one isolated level at 0, and quasidegenerate pairs at $\pm (5.3686, 6.8491)D$, $\pm (16.95728, 17.12642)D$, $\pm$

$(30.48692, 30.49622)D$, $\pm (46.16872, 46.16898)D$, $\pm (63.93715, 63.93715)D$. The observed degeneracies of the levels are accidental, and also for the two pairs for which it seems to be so it is only matter of the number significant digits. Any pair of quasidegenerate states on the top of the barrier is an admixture of odd and even $|M_S\rangle$ states. Therefore the states of a pair can be considered as orthogonal to each other, in contrast to the quasidegenerate states in the lower part of the barrier. What is certainly real is the symmetrical disposition around 0.

It is apparent that the larger $|M_S|$ the smaller the splitting. For these levels the description of the splitting as tunnel splitting is appropriate. It must be remembered here that the tunnel splitting is zero for systems with half integer S as the transverse term of the anisotropy [Eq. (8)] does not admix the ground states. These states are degenerate as predicted by the Kramers theorem,[34] according to which the minimum possible degeneracy of the states of odd-integer spin systems is two. Therefore, in principle, no tunneling is possible for a system with half-integer spin in rigorously zero field.

The split levels can, to a good approximation, be expressed as Equations (9a,b) where the $|s^*\rangle$ functions are localized states provided by perturbation theory at orders lower than S.[26]

$$|0\rangle = [|-10^*\rangle + |10^*\rangle]/\sqrt{2} \tag{9a}$$

$$|1\rangle = [|-10^*\rangle - |10^*\rangle]/\sqrt{2} \tag{9b}$$

In fact the calculation of the tenth-order perturbation may be very difficult, and an intermediate possibility is that of including perturbation say up to fourth or sixth order to have an acceptable approximation to the ground state. The amplitudes of the wavefunctions given in Equations (9) are very small through the potential barrier and large on both sides. This situation is similar to the conditions met in the tunneling of a proton in a hydrogen bond.

Tunneling may occur not only between the lowest-lying states $M_S = \pm S$, but also between pairs of degenerate excited states.[35–41] This phenomenon is called the phonon-assisted (or thermally activated) tunneling mechanism, as phonons need to be adsorbed to populate the higher M_S states involved in the tunneling process. This mechanism is very important at intermediate temperature because the tunneling frequency is expected to increase on decreasing $|M_S|$. It offers therefore a shortcut for the relaxation of the molecules. In principle a molecule may not need to go over the maximum of the barrier even at relatively high temperatures, but may find a shortcut and tunnel (Figure 5).

The process of phonon-assisted tunneling relaxation is more complex then depicted in Figure 5. It has indeed some analogies with an electric circuit[37,38] with the transition probability represented by resistances/impedances and the population of the $|M_S\rangle$ states represented by voltages. There are many paths for the current to flow through the circuit just as there are many paths for the system to relax, but some of them contribute very little to the overall process. Moreover, their contribution changes with the temperature because the
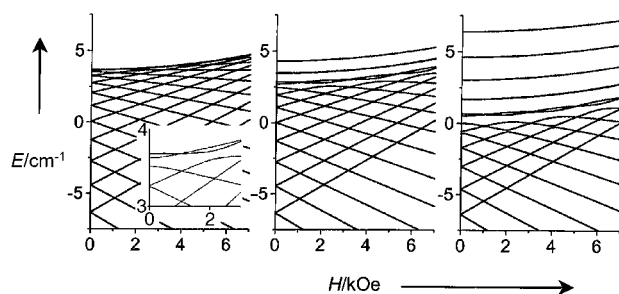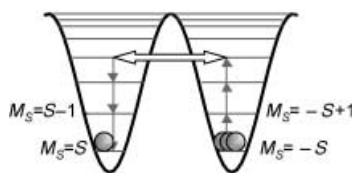

Figure 4. Energy levels for a spin state $S = 10$ as a function of an axial magnetic field. Left: $E/D = 0.01$; center: $E/D = 0.1$; right: $E/D = 1/3$, $D = 0.1$ cm^{-1}.

Figure 5. A possible "short cut" to magnetic relaxation through tunneling between thermally activated states.

population of the states as well as the phonon spectrum changes. A clearly visible effect of this admixed process is the fact that the height of the barrier experimentally measured for Mn12ac is smaller than that calculated as the energy difference between $E(0)$ and $E(-10)$.

In a coherent tunneling process the wavefunction, which initially is prepared to correspond to the localized $|-10^*\rangle$ state, should indefinitely oscillate as in Equation (10).

$$|\Psi(t)\rangle = |-10^*\rangle \cos(\omega_T t) + |+10^*\rangle \sin(\omega_T t) \qquad (10)$$

In incoherent tunneling on the other hand the spin goes from the $|-10^*\rangle$ state to the $|10^*\rangle$ and stays there. In this process energy is exchanged with the environment. The damping of the oscillations described by Equation (10) must be associated[42] with: 1) the dipolar interaction of the spins of one molecule with those of the other molecules, 2) the interaction of the electron spins with nuclear spins present in the molecule. The dipolar interactions produce fields of a few-hundred Oersted. The hyperfine interactions depend on the nature of the nuclei present in the molecule. For instance, in Mn12ac there are twelve ^{55}Mn nuclei, each with spin $I = {}^5/_2$. These may give rise to fields of a few-hundred Oersted.

The low symmetry effects in a given multiplet will be limited to the terms of Hamiltonians in Equations (2) and (8) only if the S value is smaller than 2, otherwise other even-order terms must be added to the Hamiltonians. The first higher-order terms to be introduced are the fourth-order ones.[28] For a spin $S = 10$, in principle, all the even-order terms up to 20 should be included. It is clear that the number of parameters to be introduced in this way becomes absolutely impossible to control, and quite often a conservative approach is used, in which only the minimum number is used. In general one starts with the second-order terms, then, if some experimental data cannot be fit, the fourth-order terms are added. We are aware of only one case where terms higher than four have been explicitly taken into account.[43,44] The higher-order terms take a standard form, which can be used also for the second-order terms, using the so-called Stevens operator equivalents $\Sigma_{n,k} B_n^k O_n^k$ [28] where the B_n^k are parameters to be obtained from the analysis of experimental data and O_n^k are operators of power n in the spin angular momentum. The value of k is restricted to $0 \le k \le n$. The k values to be included depend on the symmetry of the system and on the quantization axes used to define the basis set. For tetragonal symmetry $k = 0$ and 4 are allowed, for trigonal symmetry $k = 0$ and 3. For C_2 symmetry $k = 0, 2, 4$ will be needed. The k index operators couple M_S states differing by $\pm k$. The operator equivalents of the fourth order are given in the Appendix.

Contrary to the second-order terms the fourth-order terms give rise to a splitting of the S multiplets even in cubic symmetry. The $k = 0$ term does not remove the degeneracy of the $\pm M_S$ levels, but simply changes the separation between neighboring levels. The $k = 4$ terms tend to remove the degeneracy of the $\pm M_S$ levels, introducing a 45° asymmetry in the xy plane. A positive value for B_4^4 places the hard axis along x and y, while a negative value places it along the bisectors of the principal axes. In trigonal symmetry the low-symmetry component has $k = 3$ and the easy axes are found every 60°.

5. Tunneling in Magnetic Fields

If a magnetic field is applied parallel to the z axis the energies of the M_S levels change rapidly, with a slope equal to $M_S g \mu_B$ (Figure 4). It is apparent that the pairs of $\pm M_S$ levels will no longer be degenerate, and the conditions for tunneling will be lost. However, since the energy of the $+M_S$ level increases and that of the $-M_S + n$ level decreases, they will have to meet somewhere, restoring the conditions for resonant tunneling. The field at which this occurs, for axial symmetry and considering only second-order anisotropy terms, is given by Equation (11) where $D' = D/g\mu_B$, and $n = 0, 1, 2\ldots$

$$H_z(n) = n D' \qquad (11)$$

It is easy to show that if only the axial second-order ZFS parameter is included, all the $+M_S$ levels will cross the $-M_S + n$ levels at the same field. This is no longer true if higher-order terms are included.

Another interesting feature is provided by the behavior of the lowest-lying levels under the influence of a magnetic field applied parallel to the hard axis. Let us focus on the lowest-lying $M_S = \pm 10$ levels. If their separation from the other excited states, starting from the $M_S = \pm 9$ levels, is large compared to the Zeeman energy, their splitting in a field applied parallel to the hard axis will be very small. However, if one enlarges sufficiently the energy scale of the lowest-lying levels a characteristic oscillatory behavior is noticed (Figure 6).[45–47] At zero field the two levels are split by an amount, which depends on the E/D ratio. For the maximum value $|E/$
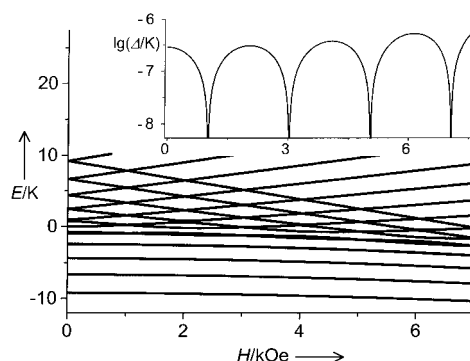

Figure 6. Energy levels of a spin state $S = 10$ in the presence of a transverse magnetic field applied parallel to the hard axis. The inset shows the tunnel splitting of the lowest $M_S = \pm 10$ pair. The curves are calculated with $D = -0.1$ cm^{-1} and $E/D = {}^1/_3$.

274

Angew. Chem. Int. Ed. **2003**, *42*, 268–297

$D| = {}^1/_3$ the separation is $2.876 \times 10^{-6}\,|D|$. The splitting rapidly decreases and goes to zero for $H_x = \sqrt{E'(E' + D')}$, where $E' = E/g\mu_B$, and $D' = D/g\mu_B$. Then it increases again, goes to a maximum at $H_x = 2\sqrt{E'(E' + D')}$, then to a minimum (zero), and so on. The oscillations are repeated S times, and beyond $H_x = (2S+1)\sqrt{E'(E' + D')}$ the oscillatory behavior is quenched. If the analogous plot was reported for the M_S level the oscillations would be observed M_S times. In general the fields at which the tunnel splitting is quenched are given by Equation (12) where $n = 0, 1, 2,..., S$.

$$H_x(n) = (2n+1)\sqrt{E'(E' + D')} \tag{12}$$

If the energy of the states is calculated in the presence of a field parallel to the z axis (the intensity $H_z(1)$ of which is defined by Equation (11)), the $(10,-9)$, $(9,-8)$, ... pairs of energy levels will be quasidegenerate for $H_x = 0$. If the transverse field H_x is applied together with a $H_z(1)$ field the oscillatory behavior is also observed, but the points of the maxima and minima are shifted by half a period. In fact if n is even the fields at which the tunnel splitting is quenched are given by Equation (12), while for odd values of n they are given by Equation (13).

$$H_x(n) = 2n\sqrt{E'(E' + D')} \tag{13}$$

These parity effects have been predicted to be detectable in mesoscopic magnets,[26,45–50] but they were experimentally observed for the first time in SMMs (see Section 6).[51]

6. Quantum Phenomena Starting from Classical Physics

Up to now we have used what can be called a molecular approach, which means we have calculated the energies of the spin levels using quantum mechanics. However, we are also interested in investigating the transition from the realm of quantum mechanics to classical physics, therefore it is interesting to also use the opposite approach, seeing if it is possible to describe quantum phenomena from a classical starting point. A more classical approach and its analytic solutions have an important advantage over the quantum mechanical one and the associated numerical methods: it provides a simpler language. While an exhaustive treatment is not the scope of this review and also it overwhelms our capabilities, a description of the oscillatory behavior of the tunnel splitting using a semi-classical approach demonstrates the advantages of the semi-classical method.[31]

The basis to do that is to use Feynman's path-integral formulation of quantum mechanics. The evolution of a system from a state x' to a state x'' can be represented as a path integral [Eq. (14)][52] where the integration is done over all the allowed paths $x(t)$, $D[x(t)]$ is defined by the discrete version of the path integral, and $S[x(t)]$ is the classical action defined through the classical Lagrangian.

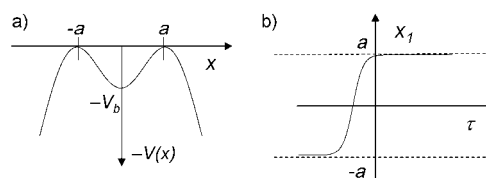$$I = \int D[x(t)] e^{(i/\hbar)S[x(t)]} \tag{14}$$

Figure 7. a) Reversed double-well potential for the imaginary time formalism; b) classical instanton solution. Modified from ref. [52].

In this formalism the tunneling of a system characterized by a two-well potential with $x'' = a$ and $x' = -a$ (Figure 7a), is made possible by introducing an imaginary time $t = i\tau$. In this way "classical" paths, $x_1(\tau)$, become possible (Figure 7b). These solutions are called instantons, because they differ from the asymptotic values $\pm a$ only for a certain "instant" of time. Evaluation of the path integral requires that all instanton solutions, $x_1, x_2, ..., x_n$, are taken into account.

The use of the Feynman's approach for a single spin is not straightforward, because there is no obvious coordinate or momentum representation for a spin, however, one commonly used procedure is that of using a transformation into canonical coordinates with subsequent use of configuration or phase-space path integral. In this way the tunnel behavior is described by the phase difference between two equivalent paths.

The instanton description has been used[51,53] to describe the tunnel splitting of a molecular cluster, such as Fe8 (see Section 8). It is assumed that the cluster has a large axial anisotropy with a strong transverse component, which makes x the hard axis. If the magnetization is prepared by saturating along $+z$ axis, when the field is switched off the system must return to equilibrium by switching to the $-z$ axis. The rotation will occur preferentially in the yz plane, and it can be either clockwise or anticlockwise. When a transverse field is applied, the two minima A and B are still connected by two paths, which depend on the strength of the transverse field and its orientation in the xy plane (Figure 8). If the two paths are covered in phase there will be a reinforcement and a tunnel splitting will result, while if they are dephased by $\pi/2$ then the splitting will be quenched. These topological interferences are also known as Berry phases.[54]
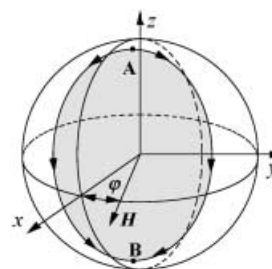

Figure 8. Unit sphere showing the classical reversal of spin. The *x, y,* and *z* axes are the hard, intermediate, and easy axis, respectively. The spins point toward $\pm z$ in zero field. The two degenerate minima A and B (the position of which depends on the transverse field) are connected by two paths, clockwise and anticlockwise. When the shaded area corresponds to $k\pi/S$ ($k = $ odd integer) the two paths give destructive interference. Modified from ref. [51].

Another approach widely used for describing mesoscopic quantum tunneling is the so-called Wentzel–Kramers–Brillouin (WKB) approach.[55–59] This is an approach to find a semi-classical approximation to the solution of the quantum-mechanical Schrödinger equation and in particular how to find its eigenstates. A modified version of this approach has been used by Villain et al.[26] where the ground-state wavefunctions for a giant spin S in biaxial-type magnetic anisotropy are approximated in the limit of a high barrier, by assuming that the states can be effectively described only by admixing states belonging to the same well (see Figure 3).

7. Mn12ac and Single-Molecule Magnets

7.1. Structure and Magnetism of Mn12ac

The synthesis and the structure of the first SMM was reported by Lis[21] in 1980. The actual formula of the compound is $[Mn_{12}O_{12}(CH_3COO)_{16}(H_2O)_4] \cdot 2 CH_3COOH \cdot 4 H_2O$. The possibility of formation of dodecanuclear manganese acetate complexes had been suggested[60] as early as 1921 but it was only when X-ray structure determination became routine that it was possible to clearly confirm the structure (Figure 9). The crystal has tetragonal symmetry (space group $I\bar{4}$) and the dodecanuclear cluster has S_4 symmetry. It was poetically described as resembling a snowflake,[21] but the tetragonal symmetry of course is not appropriate to snowflakes. Since the molecule has tetragonal symmetry there are three independent manganese ions, namely two manganese(III) and one manganese(IV), which are octahedral coordinated (Figure 10). The manganese(III) ions can be easily recognized by the bond lengths and by the elongated structure typical of these Jahn–Teller distorted ions. The
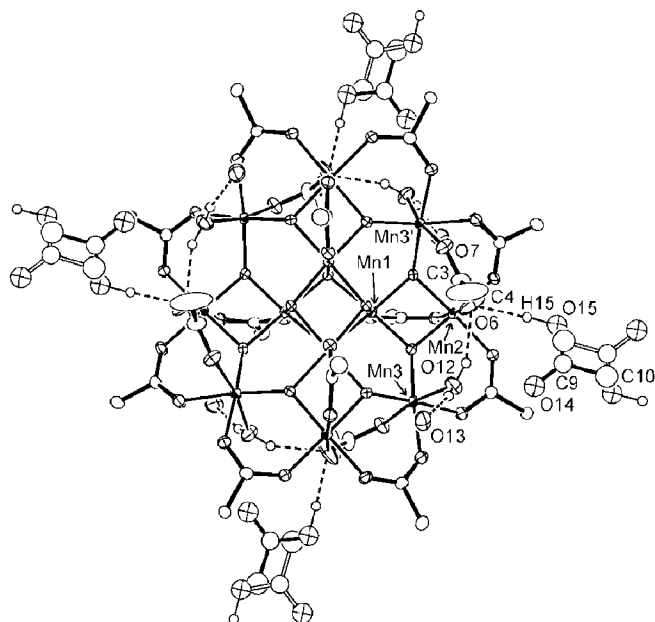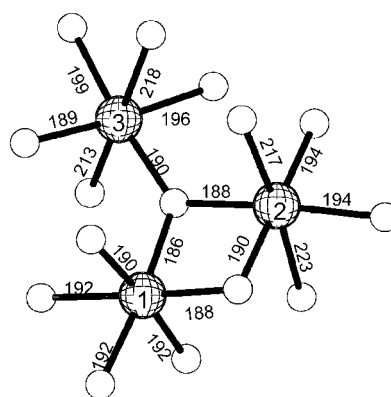

Figure 10. Coordination environment of the three independent manganese ions in Mn12ac. The labeling scheme is given in Figure 9.

structural evidence is for a mixed-valence compound belonging to the Class I of the Robin and Day[61] classification. This assignment is further corroborated by the bond valence sums,[62] which are close to 4 and to 3, respectively, for the two types of ions. Mn1, which corresponds formally to an Mn^{IV} center, is coordinated to five oxo ligands and to one oxygen atom of an acetate group; Mn2, which corresponds to an Mn^{III} center, is bound to two oxo ligands and to four oxygen atoms of acetate molecules, while Mn3, which is also formally an Mn^{III} center, is bound to two oxo ligands, three oxygen atoms of acetate molecules, and a water molecule. All the oxo ligands form μ_3 bridges. The manganese(III) ions show the typical elongated octahedral coordination seen in most Mn^{III} complexes. The elongation axis of Mn2 makes an angle of 11° with the tetragonal axis, while that of Mn3 makes an angle of 37°. These values are important for the barrier to the reorientation of the magnetization as will be discussed below.

Another important feature of the structure is the presence of acetic acid and water molecules of crystallization. Thermogravimetric studies[21] showed that loss of solvated molecules starts at 308 K and continues up to 463 K. Above this temperature decomposition of the compound sets in. The acetic acid molecules of solvation lie between adjacent clusters and close to a twofold axis and are therefore statistically distributed between the two symmetry-equivalent positions. They are at hydrogen-bond distances from the coordinated water molecules and the acetate ligands, as shown by low-temperature neutron diffraction studies.[63] In the original crystal structure solution of Lis[21] there was some disorder which has recently been well characterized[64] (Figure 9) thanks to a low-temperature (83 K) X-ray data collection. The main effect of the disorder is to reduce the real symmetry of most molecules present in the crystals; the relevance to the tunneling behavior is discussed in Section 7.2.

Several other carboxylate compounds were prepared, as shown in Table 1. The acetate derivative **1** is obtained by addition of permanganate to a solution of $Mn(CH_3COO)_2 \cdot 4 H_2O$ in water/acetic acid (2:3) through the reaction given in Equation (15).
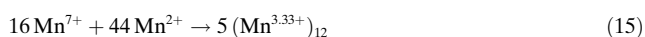

Figure 9. ORTEP view of $[Mn_{12}O_{12}(CH_3COO)_{16}(H_2O)_4] \cdot 2 CH_3COOH \cdot 4 H_2O$. The two symmetry related disordered acetic acid molecules are differentiated through full and empty bonds. Modified from ref. [64].

$$16 Mn^{7+} + 44 Mn^{2+} \rightarrow 5 (Mn^{3.33+})_{12} \qquad (15)$$

276

Angew. Chem. Int. Ed. **2003**, *42*, 268–297

Table 1: Mn12 derivatives with reported structures.[a]

Compound	R	x	Space group	Solvent molecules	Water coordination	Ref
1	Me	4	$I\bar{4}$[b]	2 CH_3COOH, 4 H_2O	1:1:1:1	[21]
2	Et	3	$P1m$	4 H_2O		[125]
3	Et	3	$P2_1/c$			[125]
4	Me, Et	4	$I4m$	2 H_2O, 4 C_2H_5COOH	1:1:1:1	[143]
5	tBuCH$_2$	4	$P1m$	CH_2Cl_2, CH_3NO_2	1:2:1:0	[139]
6	Ph	4	$P1m$		2:2:0:0	[65, 141]
7	Ph	4	$Fdd2$	2 C_6H_5COOH	2:2:0:0	[142]
8	p-Me-C$_6$H$_4$	4	$C2/c$	p-Me-C$_6$H$_4$COOH	1:2:1:0	[125]
9	p-Me-C$_6$H$_4$	4	$I2/a$	3 H_2O	1:1:2:0	[125]
10	p-Cl-C$_6$H$_4$	4	$C2/c$	8 CH_2Cl_2	2:2:0:0	[125]
11	m-Cl-C$_6$H$_4$	3	$P1m$	m-Cl-C$_6$H$_4$COOH	?	[144]
12	o-Cl-C$_6$H$_4$	4	$Pnn2$	CH_2Cl_2, 5 H_2O	1:1:2:0	[140]
13	PhCH$_2$	4	$P1m$		1:2:1:0	[139]

[a] General formula $[Mn_{12}O_{12}(RCOO)_{16}(H_2O)_x]\cdot S$. [b] Site symmetry S_4.

The reaction has an excellent yield (typically 80 %). The preparation is similar to that used for preparing manganese(III) acetate, which is a polymer containing trinuclear units which are suspected to be involved in the mechanism of formation of the cluster.

The other carboxylate compounds are generally obtained by treating a slurry of the acetate derivative in a suitable solvent with the desired carboxylic acid. A typical reaction is that described for the preparation of the benzoate derivative.[65] Treatment of Mn12ac with a 100% excess of benzoic acid in CH_2Cl_2 leads to a majority, but not all, of the acetate ligands being exchanged. The black solid obtained, which contains both acetate and benzoate, is further treated with a tenfold excess of benzoic acid to give the completely substituted derivative.

The interesting feature of the class of Mn12 clusters is that they remain intact in solution, as shown by proton NMR spectroscopic measurements on the acetate, propionate, and benzoate derivatives.[66] A broad concentration-dependent peak in the spectrum of Mn12ac is assigned to the weighted average of bound and free water molecules, which indicates that the ligand exchange is fast on the NMR time scale. There are only three other resonance signals, which correspond to the three magnetically inequivalent acetate ions, of relative intensity 1:1:2, which indicates that the tetragonal symmetry of the crystal is preserved in solution. The two resonance signals which are most shifted downfield are assigned to the acetate ligands bridging the Mn^{3+} ions, while the upfield peak is assigned to the acetate groups bridging the four Mn^{3+}–Mn^{4+} pairs. The signal of double intensity is assigned to the equatorial acetate groups.

The temperature dependence of $\chi_m T$ for a polycrystalline powder sample of Mn12ac is shown in Figure 11. At room temperature its value (19.4 emu mol^{-1}K) is smaller than expected for uncoupled spins (31.5 emu mol^{-1}K). This result indicates an overall antiferromagnetic coupling. On decreasing temperature $\chi_m T$ goes through a minimum indicating ferrimagnetic behavior as a result of antiferromagnetic interactions with no compensation of the individual magnetic moments. The increase in $\chi_m T$ on further decreasing temperature gives rise to a broad maximum at approximately 55.6 emu mol^{-1}K, which is close to the value expect-

ed for a spin $S=10$ (55 emu mol^{-1}K), but very far from the value expected for ferromagnetic coupling ($S=22$; 253 emu mol^{-1}K), which confirms that the cluster has a ferrimagnetic spin arrangement. The decrease of $\chi_m T$ at lower temperatures may indicate a large zero-field splitting of the ground state or inter-cluster interactions. The former hypothesis has been independently confirmed through many different experimental techniques.

The first unambiguous evidence of the ground $S=10$ state came from high-field (HF) magnetization studies.[19] Single-crystal magnetization data provided evidence of a very large easy-axis magnetic anisotropy (Figure 12).[67] Both the parallel (to the tetragonal axis) and perpendicular magnetization reach a saturation value of about 20 μ_B, as expected for an $S=10$ state. However the former curve increases much more rapidly than the latter, indicating a strong Ising anisotropy.

The anisotropy has been confirmed by HF-EPR spectroscopy (Figure 13) on a polycrystalline powder at variable temperature at a frequency of 525 GHz, in applied fields up to 26 T.[19, 68] Since the Zeeman energy becomes comparable to
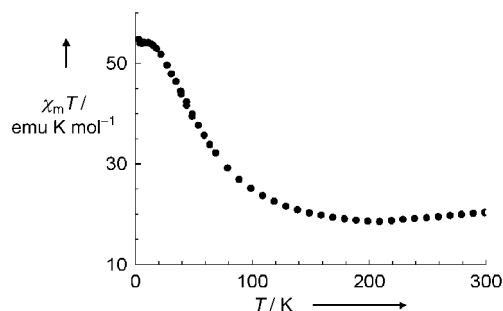

Figure 11. Temperature dependence of $\chi_m T$ for a polycrystalline powder of Mn12ac.
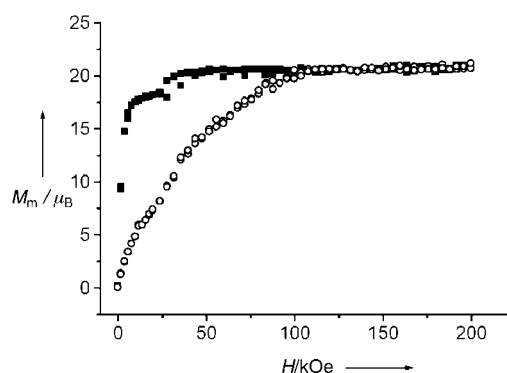

Figure 12. High-field magnetization curves for a single crystal of Mn12ac: ■ magnetic field parallel to the tetragonal axis; ○ magnetic field perpendicular to the tetragonal axis. Modified from ref. [67].
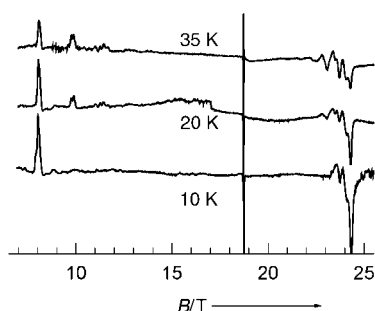
Angew. Chem. Int. Ed. **2003**, *42*, 268–297

277

Figure 13. 525 GHz EPR spectra of a polycrystalline powder of Mn12ac at different temperatures. The narrow signal marks the $g = 2.00$ resonance.

kT at low temperature, strong depopulation effects are indicated by the HF-EPR spectra, with certain lines disappearing on decreasing temperature.[69] The features appearing at low temperature correspond to transitions between the lowest $M_S = -10$ and the first excited $M_S = -9$ levels. The experimental spectra show that the features observed at low field correspond to resonances of crystallites with the tetragonal axis parallel to the applied magnetic field, while those at high field correspond to crystallites with the magnetic field perpendicular to the tetragonal axis (i.e., in the tetragonal plane). The separation between two neighboring parallel lines should be equal to $2D/g_e\mu_B$ (where D is the parameter defined in Equation (2), Section 3). Actually the separation between pairs of neighboring lines is not a constant, which indicates that the higher-order terms of the anisotropy play some relevant role here. Single-crystal EPR measurements at different frequencies have also been reported[68] and the values of the parameters are given in Table 2. Similar values were also obtained through high-field magnetic torque measurements.[70] Two sets of values were obtained in different laboratories by using HF-EPR spectroscopy.[71] In general there is good agreement between the different sets, the major differences being on the transverse fourth-order terms, which are the most difficult to determine experimentally. A more troublesome problem, however, is the use of different Hamiltonians for interpreting the experimental data. In fact, many different forms of Hamiltonian have been used, often with the same symbols having different physical meanings. We have used the D and E parameters [Eq. (2), (3)] for the second-order terms and the Steven's operator equivalents O_n^k which are listed in the appendix, with the corresponding parameters B_n^k. It must be stressed that the value of the D parameter may be different if the fourth-order parameters are included in the fit. The O_4^0 operator also contains S_z^2 terms [Eq. (16)]. Therefore when the fourth-order term is included the S_z^2 operator is associated with the parameters $D - [30S(S+1) - 25]B_4^0$, whereas if only

the second-order operators are taken into consideration it is associated with D alone.

$$O_4^0 = 35S_z^4 - [30S(S+1) - 25]S_z^2 - 6S(S+1) + 3S^2(S+1)^2 \qquad (16)$$

Inelastic neutron scattering is another important tool for obtaining experimental information on the spin structure and spin excitations.[72] It is a zero-field experiment; therefore the g value of the spin system is not important. Transitions between levels following the selection rules $\Delta M_S = 0, \pm 1$ are allowed. High-resolution spectra of Mn12ac[73,74] (Figure 14) show that the experimental spacing of the levels is not regular; this is then an experimental indication that fourth-order terms must be introduced.

Another technique has recently become available for the measurement of the energy spacing of spin levels in zero applied magnetic field, namely a quasi-optic submillimeter backward-wave-oscillator (BWO) technique.[75] The BWO technique is operated in the frequency-scanning mode. The scanning is carried out at different points by varying the BWO supply voltage in steps. The frequency resolution of the apparatus $\Delta\nu/\nu$ is 10^{-4}–10^{-5}. Three transitions were observed[76] in the frequency range 0–35 cm^{-1}, which correspond to the transitions $\pm 10 \to \pm 9$, $\pm 9 \to \pm 8$, and $\pm 8 \to \pm 7$. Also in this case the irregular spacing of the levels confirmed the need of fourth-order terms.

The above spectroscopic techniques show some additional features, other than the features which can be safely assigned to transitions within the $S = 10$ ground state. These extra features have been assigned either to minority species present as unavoidable defects in the crystals or to transitions involving the lowest-lying excited states ($S = 9, 8, \ldots$). While crystal defects are now well known, the evidence for transitions involving levels other than $S = 10$ is far from conclusive.

Specific-heat measurements provided[67,77] no evidence for long-range order in the compound, thus ruling out intercluster interactions as the origin of the deviation of the χT values from those expected for $S = 10$.

The $S = 10$ ground state can be modeled at the simplest level by assuming that all the manganese(III) spins are up and the manganese(IV) spins are down. Polarized neutron-diffrac-
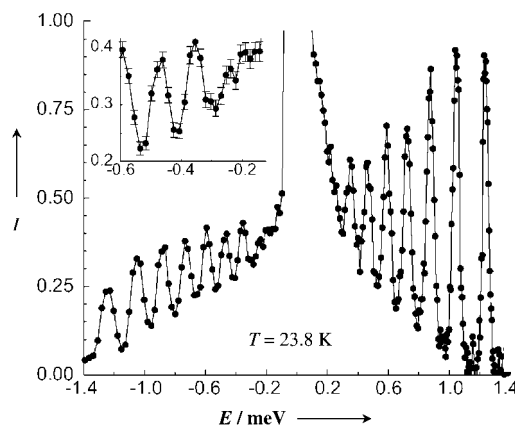
Table 2: Zero-field splitting parameters for Mn12ac in cm^{-1}.

D	B_4^0	B_4^4	Lit.
$-0.46(2)$	$-2.2(2) \times 10^{-5}$	$\pm 4(1) \times 10^{-5}$	[68]
$-0.457(2)$	$-2.33(4) \times 10^{-5}$	$\pm 3.0(5) \times 10^{-5}$	[73]
-0.47	-1.5×10^{-5}	-8.7×10^{-5}	[71]
-0.46	-2.19×10^{-5}	$-$	[76]

Figure 14. Inelastic neutron-scattering data obtained for Mn12ac at 23.8 K. The inset shows the low-energy range. Modified from ref. [73].

278

Angew. Chem. Int. Ed. **2003**, *42*, 268–297

tion experiments performed on a single crystal confirmed this view.[78] Even if the calculated total magnetic moment for $S = 10$ agrees with the $20\,\mu_B$ saturation value found, the spin density on each metal center is significantly reduced compared to the spin-only value. Such a trend was indeed predicted by density functional theory (DFT) calculations.[79,80] No significant spin density was found on nonmetal atoms.

Since Mn12ac is a ferrimagnetic cluster, excited spin levels with $S > 10$ must be present. In principle these levels may become populated at high field, because in the limiting condition of a strong field the ferromagnetic $S = 22$ state must become the ground state. Clearly high fields are needed to stabilize the high-spin states, because relatively strong exchange interactions binding the spins must be overcome. Recently extremely high pulsed fields have become technically possible. An experiment reaching 800 T showed a series

of crossovers from $S = 10$ to $S = 11$, 12,…, up to $S = 22$.[81] The crossover points are observed for fields ranging from 300 to 600 T.
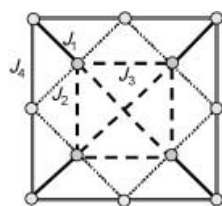
Several attempts have been made to calculate the complete spectrum of the spin levels of Mn12ac.[65,82,83] The task is far from simple, because the total number of spin states is one hundred million! Initially several attempts were made by using some ad hoc assumptions. For instance it was assumed that the J_1 coupling constant, defined in Figure 15, corresponding to the interaction between manganese(III) and manganese(IV) centers mediated by a double oxo bridge, is strongly antiferromagnetic.[65] The coupling constant J_2 is between manganese(III) and manganese(IV) ions mediated by a single oxo bridge, J_3 is that between manganese(IV) ions, while J_4 corresponds to the exchange between the manganese(III) ions, and the Hamiltonian used is in the form $\mathscr{H}_{ex} = J\mathbf{S_a}\mathbf{S_b}$.

Figure 15. Scheme for calculating the spin states of Mn12ac.

It may be assumed that the four Mn^{III}–Mn^{IV} pairs connected by J_1 are in the ground $S = 1/2$ state, and that the contributions from the excited $S = 3/2$, $5/2$, and $7/2$ states may be neglected. By using this assumption sample calculations were performed, in which the constants J_2, J_3, and J_4 were varied in a relatively small range. It was observed that the S values of the calculated ground states could vary from 8 to 10, depending on the values of the parameters used.

Later the calculations were performed again trying to fit the excited states made available by the high-field experiments described above.[81] In this case, assuming that the assignment of the experimental crossover fields is correct it is possible to perform complete calculations, because in this case the energies of the highest excited states can be calculated by diagonalizing relatively small matrices.[65] The values of the parameters changed dramatically. Unfortunately these data do not allow calculation of the ground state. Tupitsyn et al. provided further sets of parameters, which showed that the previously reported parameters did not describe the $S = 10$ ground state.[82]

Recently more powerful calculation techniques have been implemented.[83] These methods use an efficient system for representing a state, in a computer, by a single number.

Further, the spatial symmetry (S_4 in the case of Mn12ac) is exploited by using the valence-bond (VB) method, which employs the Rumer–Pauling rule.[84] Using the complete set of spin states it was shown that the previous approximate calculations fail to give the correct ground state. Sample calculations showed that with $J_1 = 149\ cm^{-1}$ and $J_2 = 59\ cm^{-1}$, the spin of the ground state is very sensitive to J_4 for a fixed value of J_3. Calculation of the temperature dependence of the susceptibility provides a check for the goodness of the parameters. The chosen values of the parameters were based on the assumption of a ground $S = 10$ state with $S = 9$ lying 35 K above. In the reported calculations, with $J_3 = 59\ cm^{-1}$, $J_4 = -44\ cm^{-1}$, an $S = 11$ excited level is present at $179\ cm^{-1}$. This should give a crossover to the ground state in a field of 192 T, not too far from the experimentally determined one, 382 T. Calculations have been also performed in the Lanczos formalism,[85,86] which for a particular S value give only the lowest-lying states. The best-fit parameters $J_1 = 62\ cm^{-1}$, $J_2 = 61\ cm^{-1}$, $J_3 = 0\ cm^{-1}$, $J_4 = 12\ cm^{-1}$ were obtained and reproduce the presence of an $S = 9$ at approximately 35 K and the energies of the states with $S > 10$.

The largest contribution to the origin of the magnetic anisotropy of Mn12ac comes from the single-ion anisotropy of the Jahn–Teller-distorted manganese(III) ions. With a defined ground state, and strong exchange as a limiting condition, it is possible to express the observed zero-field-splitting parameter D as a linear combination of the single-ion zero-field splitting parameters D_2 and D_3 of the two crystallographically independent manganese(III) ions, Mn2 and Mn3, respectively.[42] If the ground state is defined by a coupling scheme in which the eight manganese(III) ions are ferromagnetically coupled to give a total spin $S_A = 16$, and the four manganese(IV) ions to give a total spin $S_B = 6$, Equation (17) holds for the ground $S = 10$ state, where $a_2 = a_3 = 0.02845$ as calculated from spin projection techniques.[33]

$$D_{tot} = a_2 D_2 + a_3 D_3 \tag{17}$$

Assuming, for the sake of simplicity, that $D_2 = D_3$, incorporating the experimental D value in Equation (17) gives $D_2 = -2.0\ cm^{-1}$, a value totally acceptable if compared to the experimental parameters observed in isolated manganese(III) complexes. Analogous relationships have been calculated for the fourth-order terms,[42] although no safe values are available for the individual ions.

To evaluate the magnetic anisotropy of Mn12ac starting from first principles treatments were attempted using DFT calculations.[79,80] These calculations start from naked $Mn_{12}O_{12}$ clusters. Rather unsurprisingly these clusters do not compare well with the structure and magnetic properties of Mn12ac. More interestingly the calculated ground state of the complete cluster is $S = 10$ as experimentally observed. The unpaired spin density is essentially localized on the manganese ions, and is negative for the inner tetrahedron and positive for the outside ring. Significant spin density is also calculated on the bridging oxo groups. On introducing spin–orbit coupling into the calculations, the second-order contribution to the barrier was estimated to be in astonishingly good agreement with the experimental data.

Angew. Chem. Int. Ed. **2003**, *42*, 268–297

279

More sophisticated phenomena have also been taken into consideration, including the contributions from spin–spin interactions to the magnetic anisotropy.[87] Among these the intracluster dipolar interactions seem to play only a minor role, while those determined by antisymmetric exchange may play a significant role. Detailed calculations have been performed assuming that J_1 is dominant.[88] To justify the experimental zero-field splitting an antisymmetric exchange contribution ranging from -1 to $+10$ cm^{-1} was included. Unfortunately no reliable estimate of this contribution is possible. Further, these calculations require that the molecule has a reduced symmetry.

A very powerful technique to evaluate the magnetic anisotropy of metal clusters is based on the crystal-field analysis of the magnetic anisotropy of the metal centers associated with the projection technique mentioned above.[89] It has been shown[90] that the magnetic anisotropy of manganese(III) ions can be predicted with a great accuracy by taking into account the crystal field generated by the ligands and by introducing the real geometry of the coordination sphere by using the angular-overlap (AO) model.[91] This is a ligand-field model[92] which uses molecular-orbital oriented e_σ and e_π parameters for each donor atom, and is particularly well suited to account for angular distortions in the ligand field. Its application to Mn12ac has been particularly useful in evaluating the effects of the disorder in the structure on the magnetic anisotropy.[93] If we look in more detail at the low-temperature X-ray crystal structure it is possible to model the disorder of the acetate ligand, bridging Mn2 and Mn3, which is induced by the presence of acetic acid molecules in two different positions, A and B (Figure 16). The site occupation factors are very close to 0.5, as for the acetic acid of crystallization, which, when present, form hydrogen bonds with the acetate ligands. The four different coordination environments of the manganese(III) ions, provided by the X-ray analysis, have been used in calculating the magnetic anisotropy with the AOM approach. The values of the e_σ and e_π parameters for each donor atom, taken from literature data,[89] have been corrected for the actual metal–ligand separation by assuming an exponential dependence. In Table 3 the results obtained from the calculation are reported. As can be seen, the interaction with the acetic acid molecule induces only minor changes in the D and E parameters as well as in the direction of the easy axis even if the effects on the deviation from tetragonal symmetry are sizeable. Six different isomeric forms of Mn12ac can thus be envisaged which differ in the number ($n = 0, 1, 4$) and arrangement of hydrogen-bound acetate ligands (Figure 17). Clearly, strict axial symmetry can be retained only in the case of a regular pattern of $n = 0$ and $n = 4$ isomers. However, this would lead to a supercell with doubled lattice constants ($a' = b' = 2a$) for which no experimental evidence has been found. The zero-field splitting parameters of the six different isomers can be easily calculated using Equation (18) where the D parameters are now substituted by tensors.

$$\mathbf{D}_{\text{tot}} = d_2 \sum_{i=1}^{4} \mathbf{R}_i^T \mathbf{D}_2^{\alpha(i)} \mathbf{R}_i + d_3 \sum_{i=1}^{4} \mathbf{R}_i^T \mathbf{D}_3^{\alpha(i)} \mathbf{R}_i \qquad (18)$$
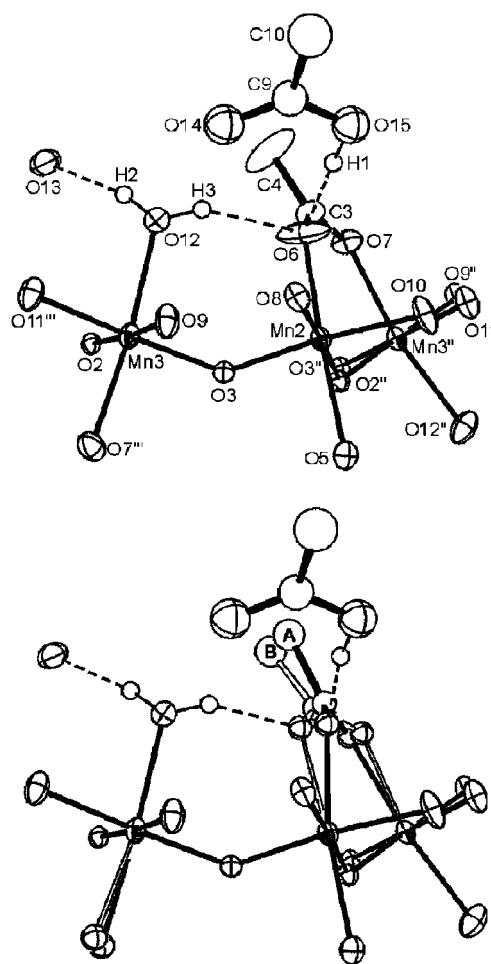

Figure 16. Coordination sphere of Mn2 and Mn3, as determined from anisotropic refinement of the displacement factors of C3, C4, O6, and O7 (top) and from an isotropic model with disorder fitting (bottom). Thermal ellipsoids are set at 50% probability. Methyl hydrogen atoms are omitted for the sake of clarity.

Table 3: Calculated Mn^{III} magnetic anisotropy parameters in Mn12ac.

Site	D [K]	E [K]	δ [°][a]
Mn2A	−4.92	0.40	11.6
Mn2B	−5.27	0.27	10.7
Mn3A	−4.57	0.10	37.2
Mn3B	−4.40	0.07	37.1
Mn3 flipped[b]	−4.64	0.06	58.4

[a] δ is the angle between the easy-axis direction of each manganese site and the crystallographic c axis. [b] The elongation axis of Mn3 has been flipped to point towards an oxo ligand (see section 7.3 and 7.5).

In Equation (18) $\alpha(i)$ describes the disorder induced by acetic acid molecules in positions A or B, $\mathbf{D}_2^{\alpha(i)}$ and $\mathbf{D}_3^{\alpha(i)}$ are the single-ion zero-field-splitting tensors for the Mn2 and Mn3 sites generated by the ith symmetry operation of the S_4 point-group. The resulting $\mathbf{D}_{\text{tot}}$ tensor turns out to be axial and diagonal in the crystal axes reference frame only for $n = 0$ and $n = 4$. In the other four cases nonzero off diagonal terms are present and diagonalization of the matrices provided the D and E parameters along with the angle θ between the easy axis and the crystallographic c axis (Table 4). The easy axis of

a) ▮ = CH₃C(O)-OH

Mn12 =

n = 0 (S₄)   n = 1 (C₁)   n = 2 "cis" (C₁)

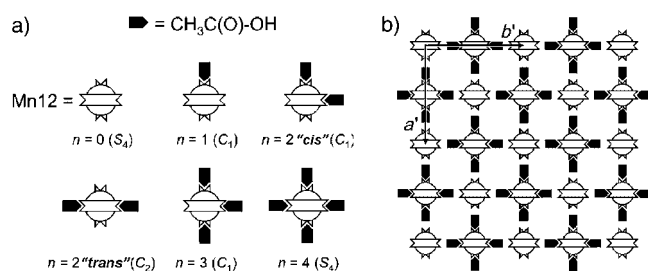n = 2 "trans" (C₂)   n = 3 (C₁)   n = 4 (S₄)

b)

Figure 17. a) The six hydrogen-bond isomers of Mn12ac; b) a possible aggregation of isomers retaining the tetragonal symmetry.
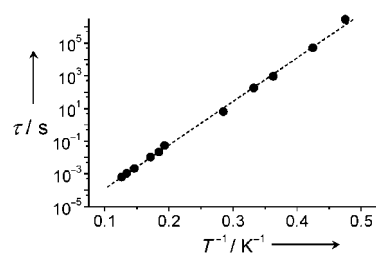

Figure 18. Temperature dependence of the relaxation time of the magnetization of Mn12ac. The dashed line corresponds to an Arrhenius law with $\tau_0 = 2.1 \times 10^{-7}$ s, $\Delta/k = 62$ K.

Table 4: Calculated magnetic anisotropy and tunnel splitting of the isomers of Mn12ac.

Isomer	c [%]	D [K]	E [K]	δ [°]	$\Delta_{-10,4}$ (n = 6)[a]
n = 0	6.25	0.759	0	0	0
n = 4	6.25	0.797	0	0	0
n = 1	25	0.769	2.34×10^{-3}	0.3	8.8×10^{-8}
n = 2, cis	25	0.778	1.87×10^{-4}	0.4	7.0×10^{-9}
n = 2, trans	12.5	0.778	4.70×10^{-3}	0	1.7×10^{-7}
n = 3	25	0.788	2.35×10^{-3}	0.3	8.9×10^{-8}
"flipped"	n.a.	0.754	4.39×10^{-2}	9.0	7.3×10^{-7}

[a] The tunnel splitting is calculated at the level crossing of $M_S = -10$ and $M_S' = 4$ corresponding to $n = 6$ [see Eq. (11)] assuming for the ZFS parameters the same as in ref. [73] but including the E term here reported in the 4th column.

the different species does not deviate significantly from the crystallographic c axis. The six species have very similar D values (within ±2%), which is in acceptable agreement with the experimental values reported in Table 2, considering the approximations involved (definition of the ground-state wavefunctions and the related projection coefficients, neglect of higher-order terms, etc.).

7.2. Slow Relaxation and Quantum Tunneling of the Magnetization of Mn12ac

The large zero-field splitting of the ground $S = 10$ provides a barrier for the reorientation of the magnetization at low temperature as explained in Section 3. If only second-order terms are included in the Hamiltonian the calculated barrier for Mn12ac is about 70 K. The relaxation time of the magnetization has been experimentally found to follow a thermally activated behavior, with $\tau_0 = 2.1 \times 10^{-7}$ s, $\Delta/k = 62$ K.[20] Figure 18 shows the temperature dependence of $\ln(\tau)$. The relaxation time becomes of the order of months at 2 K. Recent determinations suggest that below 2.0 K τ becomes slightly dependent on temperature and that at 1.5 K it is of the order of 50 years.[94]

The first evidence of slow relaxation of the magnetization came from ac susceptibility measurements (Figure 19).[19,95] In an ac experiment an out-of-phase signal, χ'', is expected to be seen if the relaxation frequency of the magnetization of the sample becomes lower than the frequency of the ac magnetic field.[27] At the temperature at which χ'' goes through a maximum the relaxation frequency of the magnetization is equal to the ac field frequency.

Since the relaxation time becomes so long magnetic hysteresis is observed.[20] Experiments performed on single crystals, with the external magnetic field applied parallel to the unique axis, showed a stepped hysteresis[96,97] as reported in Figure 20. The first reported experiment[96] was performed on a group of crystals oriented with their c axis parallel to the magnetic field. The crystals could be oriented in a high field at room temperature, taking advantage of the large shape anisotropy of the microcrystals. The origin of the steps, which is not related to the Barkhausen effect,[27] has been assigned to the thermally assisted quantum tunneling of the magnetization.[35–41] Similar conclusions had been reached on the basis of ac magnetic-susceptibility measurements.[67] The steps are observed at the fields at which pairs of levels become degenerate. They correspond to relative minima in the relaxation times, because at these fields two mechanisms are operative, namely the thermally activated and the quantum tunneling. At the fields corresponding to flat regions of the magnetic hysteresis curve the degeneracy of the levels is lost
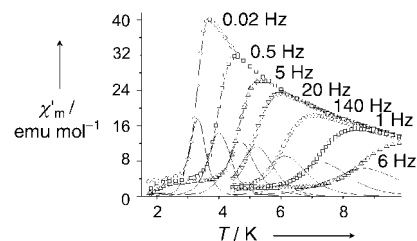

Figure 19. Temperature dependence of the in-phase ac magnetic susceptibility of Mn12ac at different frequencies.
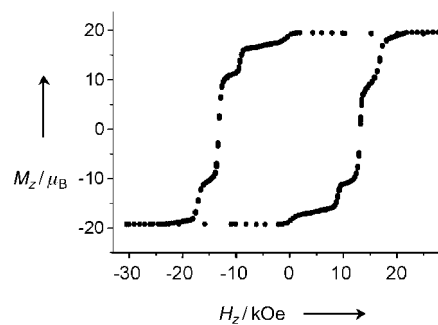

Figure 20. Magnetic hysteresis loop for a single crystal of Mn12ac with the field parallel to the tetragonal axis at 2.1 K. Modified from ref. [97].

and the tunneling mechanism is destroyed giving longer relaxation times. The field dependence of the relaxation time of the magnetization is shown in Figure 21. Many other magnetic experiments[98–103] have confirmed this picture but a similar trend has been observed using different techniques including specific-heat-capacity measurements[104–106] and NMR spectroscopy.[107, 108]

Often the final proof for quantum tunneling is associated with the temperature independence of the relaxation time. This limit is never reached experimentally for Mn12ac, because below 2 K τ becomes extremely long, and reliable measurements, which require the temperature of the experiment to be fixed for very long times become practically impossible. At low temperature, however, relaxation can be still observed if a strong axial field is applied. The relaxation in fact involves the transition from the $M_S = -10$ metastable state to M_S' states. The smaller $|M_S'|$ is the larger the applied field. The relaxation is accelerated by the reduction of the barrier height as well as by the more efficient admixing in of the states with lower $|M_S'|$. In the presence of fourth-order axial anisotropy, as for Mn12ac, the resonant tunneling occurs at different field for different $M_S \rightarrow M_S'$ pairs. It has been possible[87, 109–112] to determine which pairs of states are involved, and at which temperature the mechanism involves exclusively the metastable ground state $M_S = 10$. It has been theoretically shown[113] and recently confirmed experimentally[111] that this crossover from thermally activated to ground tunneling can be either first or second order depending on the strength of the transverse field (Figure 22). It is important to underline that all the resonance signals are observed although the tetragonal symmetry of the transverse anisotropy would require that only every fourth step (corresponding to $M_S - M_S' = 4n$) is present. The presence of second-order transverse anisotropy, which is expected in most of the Mn12ac molecules in the crystal,[93] allows $(2n)$ transitions, whereas for the odd $(2n + 1)$ transitions a transverse field must be included. More recently, an accurate analysis of the dependence of the magnetization on the sweeping rate of the axial magnetic field has shown[114] that the fractions of reversed magnetization at the even transitions scale well on a single curve if plotted as a function of a scaling parameter. This parameter is proportional to the logarithm of the inverse of the field sweeping rate. Such an experimental behavior can be justified if a broad distribution of the second-order transverse anisotropy is present. It has been suggested[115] that a small concentration (0.1 %) of disordered molecules in
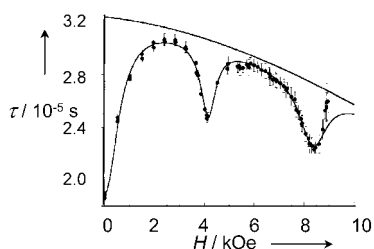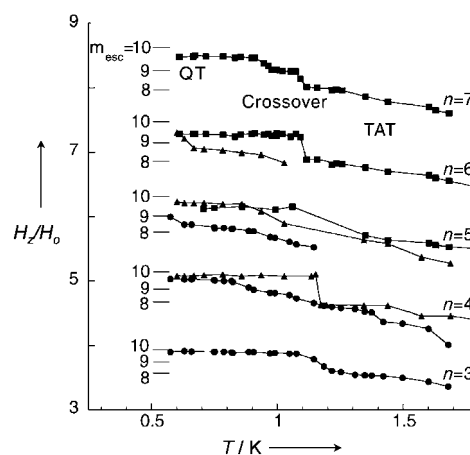

Figure 22. Temperature dependence of the peak positions in the unit $H_0 = 4.2$ kOe, $\theta = 0°$ (■), $\theta = 20°$ (▲), and $\theta = 35°$ (●). QT = quantum tunneling, TAT = thermally activated tunneling. Modified from ref. [111].

the crystal structure and the associated gradient of the magnetic anisotropy, which extends over a wide distance, can give rise to the distribution in the E parameter and the consequent scaling law. Crystal-field calculations have, however, shown that the magnetic anisotropy is only slightly affected by strong perturbation of the structure (such as, the presence of a hydrogen-bonded acetic acid molecule) and therefore long-range effects of disorder are expected to be very small.[93] On the contrary the presence of several isomers with significantly different transverse anisotropy could mimic the broad distribution required to justify the experimental behavior.

An important point to be clarified is how the relaxation times are actually measured. The most direct way, which can be used when τ is sufficiently long, is to saturate the sample (better a crystal than a powder), switch off the field, and measure the decay of the magnetization as a function of time. In the simplest case, when only one decay mechanism is possible the magnetization follows the exponential law given in Equation (4). More complex behavior is usually observed, which can be fitted with stretched exponentials [Eq. (19)] where M_{eq} and $M(0)$ are the equilibrium and initial magnetization, respectively, and β is a coefficient ranging from 0 to 1.[116, 117]

$$M(t) = M_{eq} + [M(0) - M_{eq}] \exp[-(t/\tau)^\beta] \qquad (19)$$

The stretched exponential fit has the same role as the Curie–Weiss fit of magnetic susceptibility, it takes into account all the possible deviations from simple single-exponential behavior. In Mn12ac the relaxation has been observed to deviate from single exponential at short times[94, 99] (presumably because of the dipolar interactions with the neighboring molecules), and to be accurately reproduced by a single exponential at longer times. The mechanism by which the dipolar fields determine a non-exponential decay is intuitively clear. If the sample is initially saturated, when the field is removed it will be far from equilibrium, and will start to relax. The actual field felt by a

Figure 21. Field dependence of the relaxation time of the magnetization of Mn12ac ($T = 8.5$ K) obtained from an ac susceptibility measurement at a frequency of 5.37 kHz. Modified from ref. [240].

282

Angew. Chem. Int. Ed. **2003**, *42*, 268–297

relaxing molecule will depend on the state of the neighboring molecules, each molecule feeling a different field from the others.

Sometimes the stretched exponential fit has been used for the whole set of data, alternatively the initial data are neglected and the remainder of the M/t measurement treated with the single exponential. In particular Thomas et al.[94] found that in a single crystal of Mn12ac a single exponential fit is possible above 2.8 K. Below 2.0 K the initial relaxation follows a square-root regime in Equation (20) with $M(0)$ the initial magnetization and M_{eq} the equilibrium magnetization, as anticipated for dipolar and/or hyperfine assisted tunneling, based on theoretical work by Prokof'ev and Stamp.[118,119]

$$M(t) = M(0)_{in} + ([M_{eq} - M(0)])(t/\tau)^{1/2} \qquad (20)$$

The specific heat capacity has also been used to measure relaxation times. In a series of sophisticated experiments Fominaya et al. used a nanocalorimeter[120] to measure the specific heat of single crystals of Mn12ac as a function of frequency with a magnetic field applied parallel to the tetragonal axis. The nanocalorimeter consists of a 3-μm-thick silicon membrane suspended in a vacuum and linked to the thermal bath by twelve narrow silicon bridges. A planar NbN thermometer and a CuNi heater are placed on one side of this membrane and the samples are pasted with grease on the other side. The experimental set-up permits not only the study of extremely small crystals, but also a very accurate measurement of the sample temperature. Experimentally one can measure the absolute specific heat capacity C at frequency ω [Eq. (21)] where C_{bi} is the specific heat capacity in the bilateral regime when the levels on both sides of the barrier are accessible while in the unilateral regime, when the states on the opposite side of the barrier are not accessible, the specific heat is reduced to C_{uni}.

$$|C(\omega)| = \sqrt{C_{uni}^2 + \frac{C_{bi}^2 - C_{uni}^2}{1 + \omega^2 \tau^2}} \qquad (21)$$

When $\omega\tau \gg 1$, that is, when $\tau \to \infty$, then Equation (21) becomes $C(\omega) = C_{uni}$, which means that the jumps over the potential barrier are impossible during the measuring time $2\pi/\omega$. At the other limit, $\omega\tau \ll 1$ (that is, when $\tau \to 0$), $C(\omega) = C_{bi}$, which is the equilibrium value. At the resonant fields, when the relaxation accelerates because of the tunnel mechanism, the bilateral regime is suddenly attained and the specific heat capacity increases significantly showing well resolved peaks (Figure 23).[106] Using Equation (21) it is possible to calculate the relaxation time [Eq. (22)]:

$$\tau = \frac{1}{\omega}\sqrt{\frac{C^2(\omega) - C_{bi}^2}{C_{uni}^2 - C^2(\omega)}} \qquad (22)$$

The values of the experimentally determined relaxation times as a function of an axial magnetic field are shown in Figure 24.[105] They agree reasonably well with the values
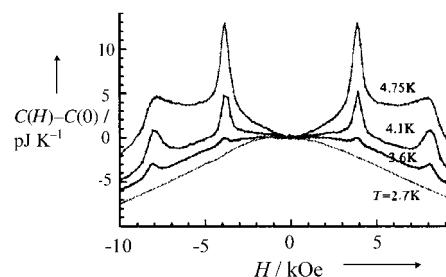
Figure 23. Field dependence of the ac specific heat (10 Hz) of a single crystal of Mn12ac. The magnetic field is applied parallel to the tetragonal axis. Modified from ref. [106].
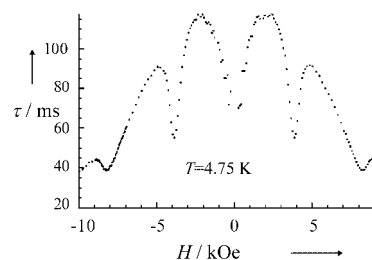

Figure 24. Field dependence of the relaxation time of the magnetization of a single crystal of Mn12ac obtained through ac specific heat capacity measurements. Modified from ref. [105].

obtained with other experimental techniques, and in particular show the wavelike behavior, with peaks and minima at $H_n = nH_0$ ($n = 0, 1, \ldots; H_0 = 0.45$ T).

7.3. Tunneling Mechanisms and Quantum Coherence in Mn12ac

All data in Section 7.2 provide a clear picture of quantum tunneling effects in Mn12ac in the thermally assisted regime. Similar theoretical results have been produced by considering the role of phonon coupling.[35,36,38–40,121] The problems for a detailed comparison with the experimental data are that acceptable values are not available for several parameters, but by and large, the theoretical picture is clear.

However, several questions are still open, such as what is the detailed relaxation mechanism at low temperature and with the limiting condition of a low transverse static field, and if it is possible to observe quantum coherence? There is no doubt that a splitting of the $\pm M$ levels is needed to observe tunneling, and there is no doubt that this splitting is small. Moreover, the selection rules imposed by the second- or fourth-order transverse anisotropy terms require that the tunneling at odd transition be quenched. Therefore other mechanisms must be available that allow the tunnel process.

Inherent sources of tunnel splitting are the hyperfine fields caused by the presence of magnetic nuclei (^{1}H, ^{2}H, ^{13}C, ^{55}Mn) and the dipolar fields caused by the presence of the other Mn12ac molecules in the lattice. Finally, it is also possible to determine a splitting of the $\pm M$ levels by using an external magnetic field applied perpendicular to the tetragonal axis. In fact the presence of disruptive external magnetic fields may be a source of error. In a single-crystal experiment it is very difficult to orient the external field
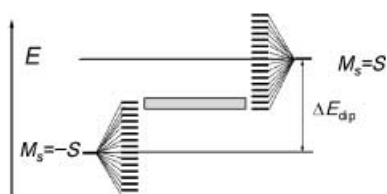
283

Figure 25. Internal dipolar fields change the energies of the two levels split by the tunnel interaction, and thus hinder tunneling. By effectively broadening the levels hyperfine interactions restore the matching of the left and right levels (shaded area).
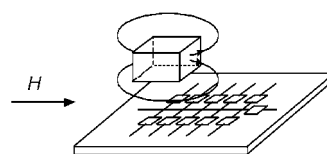

Figure 26. Schematic view of the micro-SQUID array used in the high sensitivity magnetometer. The sample is placed directly on the array. Modified from ref. [127].

exactly parallel to the tetragonal axis to provide a nonzero component in the tetragonal plane. The hyperfine field is expected to be mainly determined by the ^{55}Mn nuclei, which have $I = ^5/_2$ and correspond to the sites where the highest spin density is concentrated. The hyperfine coupling constant is typically of the order of 10 mT for manganese ions, and in fact this value is confirmed by NMR spectra (see Section 7.4.)

The tunnel splitting of Mn12ac in the ground $M_S = \pm 10$ state is very small, of the order of 10^{-10} K and thus much smaller than the dipolar and hyperfine fields. An estimation of these contributions to the ground doublet-energy separation gives a value of Δ between 0.1 and 0.5 K. Starting from simple theoretical arguments tunneling should not be observed. However, to solve this problem Prokof'ev and Stamp[118,119] suggested a theory (PS theory), according to which the dipolar and hyperfine fields, by varying the bias at each molecular site in time, can continually bring more molecules to resonance. The point can be made clearer by considering Figure 25. The rapidly fluctuating hyperfine fields bring molecules into resonance. The dipolar fields of tunneled spins can lift the degeneracy and thus remove a large number of neighboring spins from resonance. However, a gradual adjustment of the dipolar fields across the sample (up to 0.03 T in Mn12ac) caused by tunneling relaxation, brings other molecules into resonance and allows continuous relaxation. Therefore one expects a fast relaxation at short times and slow logarithmic relaxation at long times.

Looking in detail at the PS theory, the short-time relaxation of the magnetization must follow Equation (23).

$$M(H,t) = M(0) + [M_{eq}(H) - M(0)]\,[\Gamma_{sqrt}(H)t]^{1/2} \tag{23}$$

The magnitude of $\Gamma_{sqrt}(H)$, the tunneling rate derived from the square root analysis of the decay of the magnetization, is given by Equation (24) where $P(H)$ is the normalized distribution of molecules that are in resonance at the applied field H. $P(H)$ can be determined once $\Gamma_{sqrt}(H)$ is measured as a function of the field.

$$\Gamma_{sqrt}(H) \sim (\Delta_t^2/h)\,P(H) \tag{24}$$

Δ_t^2 is the tunnel splitting at the tunneling resonance. Experimental confirmation comes from micro-SQUID measurements on Mn12ac.[122] The experimental apparatus[123] is as shown in Figure 26. The sensitivity of this setup is as high as 10^{-17} emu, that is about ten orders of magnitude better than traditional SQUIDs. The magnetometer is an array of micro-

SQUIDs arranged on top of a chip. The sample is placed on top of the chip so that some SQUIDs are directly under the sample, others are beside the sample.

In these experiments a fast-relaxing minor species is monitored.[124] This species is only present in small percentage (2–4%) and is significantly different from the six isomers discussed in Section 7.1. Because of its small concentration it is undetected by X-ray analysis, however, it can be reasonably supposed that it corresponds to a dodecanuclear cluster where the elongation axis of one manganese(III) ion has flipped its direction. Such a modification has already been observed in two isomers of the *p*-methyl benzoate derivatives of Mn12ac clusters (see Section 7.5).[125] Again crystal-field calculations using the AOM approach can provide an estimation of the modification in the magnetic-anisotropy tensor of the flipped manganese centers (see Table 3). If one of these centers is present, the transverse magnetic anisotropy increases by an order of magnitude (Table 4) which provides an acceleration of the tunneling process. The experimental measurement of $\Gamma_{sqrt}(H)$ provides the normalized distribution of molecules that are in resonance at the applied field. This is done by a so-called "hole digging" procedure,[126,127] in which a fraction of molecules is allowed to relax by the tunneling process, which is only possible when the applied plus the internal field satisfy the resonance conditions. As the relaxed molecules have significantly modified their internal dipolar field, a hole appears in the field distribution of the tunnel probability. The term hole digging is used in analogy to the hole burning technique of spectroscopy, by which individual groups of molecules are addressed.[128] The experimental width of the distribution is of the order of 12 mT in the 40–300 mK range, a width comparable with the distribution of hyperfine fields. Calculations assuming reasonable values for the manganese(III) (6.9 mT) and manganese(IV) (8.5 mT) centers suggest a width of about 16 mT, in good agreement with the experimental data.[122]

The presence of quantum-mechanical tunneling therefore is well established for Mn12ac. The observation of quantum coherence on the other hand is still much more controversial.[104,129]

7.4. Characterization of Mn12ac by other Spectroscopic Methods

In addition to the spectroscopic methods used to construct the detailed map of the low-lying spin components of the ground $S = 10$ state, other spectral techniques have been used

to characterize this state. An important one is certainly NMR spectroscopy, because it gives direct access to the electron-spin–nuclear-spin interaction, which may assist the tunneling mechanism. NMR spectroscopy is sensitive to the electron spin, dominated by the so-called hyperfine interactions, and the nuclear relaxation. Worth mentioning here is the muon spin resonance and relaxation technique,[130,131] which is similar to NMR spectroscopy in that it provides a local probe which is sensitive to the electron relaxation.

^{1}H NMR spectra of Mn12ac in solution have been discussed in Section 7.1.[66] Recently it was possible to observe the [55]Mn NMR spectra[132,133] in a polycrystalline powder at 1.4 K (Figure 27). The spectrum was measured in zero applied field. It shows three resonance signals in the range 200–40 MHz. The low frequency sharp resonance signal is assigned to the four manganese(IV) centers and the two broad resonance signals at 280 and 370 MHz, to the crystallographically inequivalent manganese(III) centers. ^{1}H and ^{2}H NMR spectra at low temperature were also reported,[136] which show two resonance signals: one, essentially not shifted, assigned to the CH₃COO, CH₃COOH, and solvated water molecules, the other signal which is shifted, is assigned to the coordinated water molecules.

Using the time dependence of the Hahn-echo pulse sequence the relaxation of the magnetization was measured and compared to that obtained through specific-heat-capacity and dc magnetic measurements.[108] The echo is generated with a $\pi/2$-π pulse sequence at the resonance frequency. The typical $\pi/2$ pulse length was 3.5–4.5 µs and the delay τ between the two pulses approximately 50 µs. The experiments were performed on polycrystalline samples which were aligned with the anisotropy axis along the magnetic field by letting the sample sit at 4.2 K in a field of 1.8 T for several hours. The field was turned off and the system was given time to reach thermal equilibrium at the preset temperature. The field was turned on and the echo intensity was monitored as a function of time. The evolution of the magnetism with time could be reproduced with Equation (25) where h is the echo
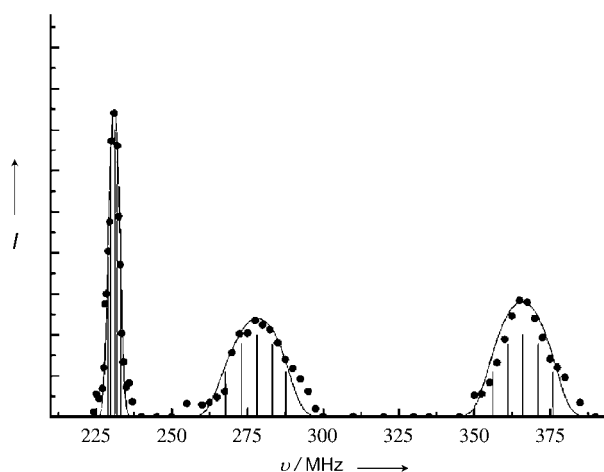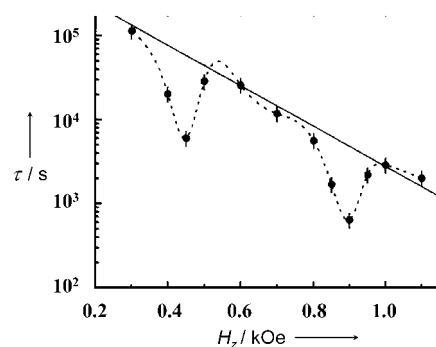

Figure 28. Field dependence of the relaxation time of the magnetization of Mn12ac at 2.4 K measured through the echo proton NMR spectroscopy. Modified from ref. [108].

magnitude and $1/W$ $(=\tau_r)$ is the relaxation time of the magnetization of Mn12ac.

$$h(t) = a[1 - \exp(-Wt)] + b \qquad (25)$$

The time dependence suggests that the nuclei feel an electronic relaxation process, following Equation (26) where N_p is the number of protons per molecule, N_m is the total number of molecules, and $N_p^{ch}(t)$ is the number of protons which undergo a change of average local field in the time interval separating the $\pi/2$-π pulses.

$$h(t) \propto [N_p N_m - N_p^{ch}(t)] \qquad (26)$$

By suitable derivation the echo height can finally be expressed as Equation (27) where N_m^{eff} is the number of molecules with protons that are affected by the local field change as a result of a molecular spin flip.

$$h(t) = h(\infty)[1 - N_m^{eff} W\tau \exp(-W\tau)] \qquad (27)$$

As $\tau = 50$ µs and W are small, Equation (27) requires that $t \gg \tau$ and $W\tau \ll 1$. The temperature dependence of τ_r in a field of 0.45 T was found to follow a thermally activated mechanism with $\tau_0 = 10^{-7}$ s, and $\Delta/k = 60$ K in acceptable agreement with the values obtained through other experimental techniques. The field dependence (Figure 28) shows the anomalies at the crossing fields described in Section 7.2.

There have been numerous other reports on the use of NMR spectroscopy with Mn12ac.[107,134–138]

7.5. Mn12 Derivatives

The Mn12 derivatives for which the structure has been reported are shown in Table 1 (Section 7.1). They all have the general formula $[Mn_{12}O_{12}(RCOO)_{16}(H_2O)_x]Y$, where Y = solvent molecules.[22] The main structural difference is the presence of either four or three water molecules in the cluster. An example of the latter category is provided by $[Mn_{12}O_{12}$-$(EtCOO)_{16}(H_2O)_3]$, which crystallizes either in a monoclinic space group, without solvent molecules, or in a triclinic space group, with four cocrystallized water molecules.[125] Also the clusters with four cocrystallized water molecules show

Figure 27. Spin echo intensity of the [55]NMR spectra of Mn12ac measured at $H = 0$ and $T = 1.4$ K. Modified from ref. [133].

significant structural differences. In all the cases the manganese(III) ions are either doubly bridged to one manganese(IV) center (type I), or singly bridged to two manganese(IV) centers (type II). The water molecules are bound to type II ions. The coordination in cluster **1** (see Table 1) is such that one water molecule per type II ion is present.[21] The manganese–water direction roughly indicates the Jahn–Teller distortion axis. In other derivatives some of the type II Mn ions have either no water molecules, or two water molecules. Four different isomers have been experimentally observed, which correspond to the coordination schemes 1:1:1:1 (as in **1**),[21,125,143] 1:2:1:0,[125,139] 1:1:2:0,[125,140] and 2:2:0:0[65,125,141,142] (the notation indicates the water coordination number of the type II Mn ions).

There are some distinctive exceptions to the rule that the oxo ligands are not found on the elongation axis. In fact, the Jahn–Teller distortion axis in **8** (see Table 1) includes one of the bridging oxo ligands, so that for this Mn center the elongation axis is approximately orthogonal to the elongation axes of the other manganese(III) centers (Figure 29).[125] In **9** the elongation axes are essentially parallel to each other.[125] The two clusters therefore can be considered as distortion isomers, as frequently observed for copper(II) compounds. It is apparent that intercluster interactions, such as hydrogen bonds, may play an important role. The magnetic properties of **8** and **9** are very different from each other.

The temperature dependence of the out-of-phase susceptibility of **8** and **9**, at different frequencies, is shown in Figure 30. It is apparent that slow relaxation effects show up at higher temperatures for **9** than **8**, which suggests a higher
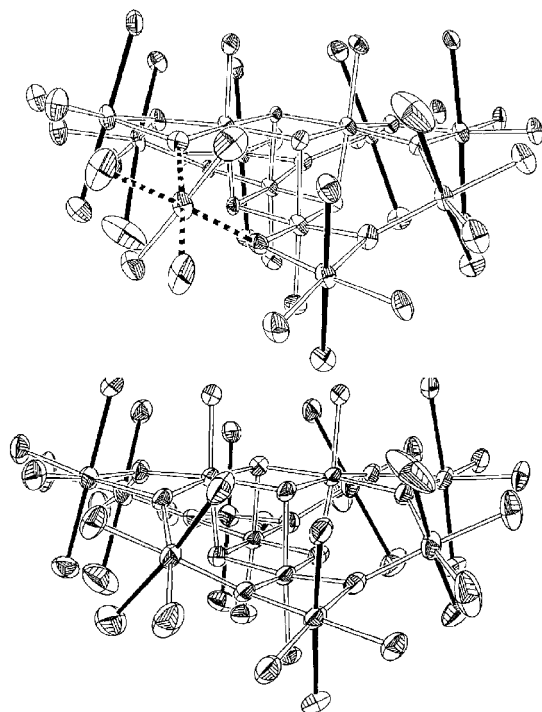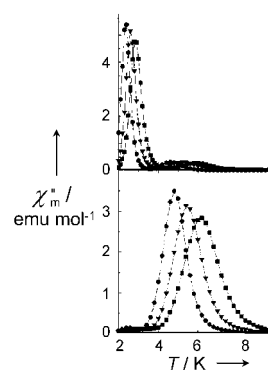

Figure 30. Plots of the out-of-phase ac magnetic susceptibility versus temperature for polycrystalline samples of **8** (upper) and **9** (lower). Modified from ref. [241].

barrier for the reorientation of the magnetization in **9**. Since the ground state in both cases is $S = 10$, the greater barrier height is associated with a larger zero-field splitting. If the zero-field-splitting parameter of the cluster depends on the projection of the individual zero-field-splitting tensors of the Jahn–Teller distorted manganese(III) center, it is apparent that the resultant must be larger in **9** (where the local distortion axes are essentially parallel to each other), than in **8** (where one of the local axes is orthogonal to the others). Distortion isomers such as these may also be responsible for the presence of two species with different relaxation properties, as frequently observed even in single crystals of Mn12 derivatives.

The compounds with three cocrystallized water molecules ($x = 3$; **2**, **3**, **11** in Table 1) have one manganese(III) center which is five coordinate.[144] The overall temperature dependence of χT is not much different from that observed in Mn12ac, but an $S = 9$ ground spin state was suggested from the analysis of the magnetization. However, a good agreement to this was only observed in the derivative with R = Ph, Y = PhCOOH·CH$_2$Cl$_2$. Several derivatives show some chemical instability, such as solvent loss, which provide ambiguity in the experimental measurements.

By treating [Mn$_{12}$O$_{12}$(RCOO)$_{16}$(H$_2$O)$_4$] derivatives with nitric acid in MeCN new compounds of formula [Mn$_{12}$O$_{12}$(NO$_3$)$_4$(RCOO)$_{12}$(H$_2$O)$_4$] (R = CH$_2$tBu, Ph) were obtained.[145] The four nitrate groups are not disordered and replace bridging carboxylate groups. The ground state is still $S = 10$, and a SMM behavior is observed at low temperature. The zero-field splitting and the barrier are very similar to those observed in Mn12ac.

7.6. Reduced Mn12 Species

From the chemical point of view one of the most exciting properties of Mn12 clusters is their stability in solution, which allows a rich redox chemistry. Differential pulsed voltammetry investigations have been reported for **1** in MeCN, which shows two reversible processes, an oxidation and a reduction, and four redox processes altogether.[65] Very similar results were observed for the benzoate derivative in CH$_2$Cl$_2$. The

Figure 29. ORTEP views of two distortion isomers **8** (top) and **9** (bottom). The elongation axes of the manganese(III) coordination sphere are indicated by filled bonds. The dashed lines indicate an unusual orientation for the elongation axis in **8**. Modified from ref. [11].
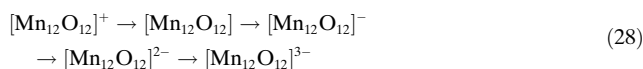
286

Angew. Chem. Int. Ed. **2003**, *42*, 268–297

oxidation process occurs at 0.79 V and the reduction process at 0.11 V. The values are referred to the Cp_2Fe/Cp_2Fe^+ ($Cp = C_5H_5$) couple. The corresponding processes are summarized in Equation (28).

$$[Mn_{12}O_{12}]^+ \rightarrow [Mn_{12}O_{12}] \rightarrow [Mn_{12}O_{12}]^-$$
$$\rightarrow [Mn_{12}O_{12}]^{2-} \rightarrow [Mn_{12}O_{12}]^{3-} \qquad (28)$$

A series of benzoate derivatives, which have similar solubility in a given solvent, allowed a comparative analysis of the role of the carboxylate group in the redox potentials.[146] It was found that the potentials satisfactorily correlate with the electron-withdrawing properties of the *para* substituent in the benzene ring. An electron-withdrawing substituent causes the carboxylate group to become less basic, reducing the electron density on the metal ions thereby making the cluster easier to reduce and concomitantly harder to oxidize.

The first reduction potential is at low enough potential that mild reducing agents, such as iodide can be used to reduce the compound. The PPh_4^+ derivatives of the clusters with R = Et and R = Ph were directly obtained by adding the iodide to the appropriate unreduced Mn12 clusters. Metathesis reactions yielded the [*m*-MPYNN]+ salt (*m*-MPYNN = *m*-*N*-methylpyridinium nitronyl nitroxide).[147] This cation is magnetic with a moment corresponding to one unpaired electron. $(PPh_4)[Mn_{12}O_{12}(Et\text{-}COO)_{16}(H_2O)_4]$ crystallizes in the monoclinic $P2_1/c$ space group.[66] The overall structure of the anion is very similar to that of the unreduced species. The reduction yielded a valence-localized species, one of the external manganese(III) ions being reduced to manganese(II). The identification of the reduced ion has been made on the basis of structural features and confirmed by bond valence sums.[62] It has been suggested that the reduction of manganese(III) rather than of a manganese(IV) ion is because the reduction of a manganese(IV) ion would introduce a distorted manganese(III) ion creating a strain in the apparently rigid $[Mn_4O_4]$ structure. The temperature dependence of the χT product is qualitatively similar to that of Mn12, which suggests a ferrimagnetic ground state, $S = {}^{19}/_2$, with a large negative zero-field splitting. The magnetic data, however, require a physically unreasonable g factor of 1.74. It is apparent that the ground spin state cannot be obtained simply by "exchanging" one of the $S = 2$ spins with a $S = {}^5/_2$ spin, because this would lead to either $S = {}^{21}/_2$, for parallel, or $S = {}^{11}/_2$, for an antiparallel alignment of this spin with those of the manganese(III) ions. A frustrated structure is dominant for $Mn12^-$, analogous to that which gives rise to $S = 9$ in Mn12. Similar results were obtained for the R = Ph derivative.

HF-EPR spectra have been used to obtain the zero-field-splitting parameter D.[146] The spectra were recorded on loose polycrystalline samples. It was assumed that a uniform orientation of the powder was achieved and the spectra were assigned on the assumption of the strong-field limit. With this simplified treatment the zero-field-splitting D was found to be -0.62 cm^{-1}. Slow relaxation of the magnetization was observed. Accurate data for the temperature dependence of the relaxation time of the R = Ph derivative showed that it follows a thermally activated pattern with $\Delta/k = 57.5$ K. The

pre-exponential factor is much larger than in Mn12ac ($\tau_0 = 3.1 \times 10^{-10}$ s). Magnetic hysteresis was also observed, with steps as observed in the unreduced compounds. A step is observed also at zero-field. If this behavior is interpreted as being a result of tunneling effects it is against the Kramers theorem, in which degeneracy cannot be removed in zero applied field. However, the dipolar fields of the other molecules may actually be responsible for this loss of degeneracy.

Recently the structure of the paramagnetic $[Fe(C_5Me_5)_2]^+$ cation and the $[Mn_{12}O_{12}(O_2CC_6F_5)_{16}(H_2O)_4]$ anion[148] have also been reported. The ground state was found to be $S = {}^{21}/_2$, with axial zero-field-splitting parameters of $D = -0.351$ cm^{-1} and $B_4^0 = -3.6 \times 10^{-7}$ cm^{-1}, as determined by HF-EPR spectroscopy.

Experiments performed with the magnetic counterion [*m*-MPYNN]+ showed much faster relaxation in agreement with the perturbation given to the cluster by the fast-relaxing radical cation.[147] No substantial change in the relaxation of the Mn_{12}^- species was observed with the $[Fe(C_5Me_5)_2]^+$ counterion.

Using carboxylate ligands with more electron-withdrawing substituents it was also possible to obtain the Mn_{12}^{2-} derivatives[149,150] [cation]$_2$[Mn$_{12}$O$_{12}$(O$_2$CR)$_{16}$(H$_2$O)$_4$], where cation = PPh$_4$, N*n*Pr$_4$, R = CHCl$_2$, C$_6$F$_5$, 2,4-C$_6$H$_3$(NO$_2$)$_2$. The second manganese(II) center (generated by the reduction of a Mn^{III} center) is also found on the outer ring. The ground state is reported to be $S = 10$, with an axial zero-field splitting of $D \approx -0.3$ cm^{-1}. Slow magnetic relaxation is observed below 7 K, in agreement with the expected reduced barrier height. Measurements performed using an array of micro-SQUID measurements showed evidence of quantum phase interference effects (see Section 8).[151] A transverse variable magnetic field parallel to the hard axis can modulate the tunnel splitting. Oscillations were observed with a periodicity of about 0.4 T.

8. Fe8

The second molecule that has been intensively investigated for its SMM behavior is commonly indicated as Fe8. The formula is $[Fe_8O_2(OH)_{12}(tacn)_6]Br_8$ (tacn = 1,4,7-triaza-cyclononane) and comprises an octanuclear cation (Figure 31).[152] The compound is prepared by the controlled hydrolysis of $[Fe(tacn)]Cl_3$ in a water/pyridine mixture in the presence of sodium bromide. The two inner iron(III) ions are octahedrally coordinated to the two bridging oxo and four bridging hydroxy ligands. Fe3 and Fe4 coordinate to three nitrogen atoms of the tacn molecules, two hydroxy and one oxo ligand, while the outer iron(III) centers (Fe5–Fe8) coordinate three nitrogen atoms and three hydroxy groups. The presence of three different Fe sites has been also confirmed by Mössbauer spectroscopy.[153,154] The oxo ligands form μ_3 bridges, while the hydroxy ligands form μ_2 bridges. Fe1, Fe2, Fe3, Fe4 form a structure which is often encountered in polynuclear metal complexes, which has been described as a butterfly structure.[155] With some fantasy Fe1 and Fe2 define the body and Fe3 and Fe4 the wings of the
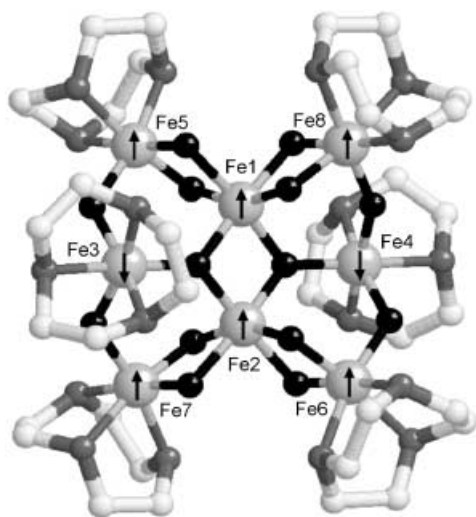
Angew. Chem. Int. Ed. **2003**, *42*, 268–297

287

Figure 31. Schematic structure of Fe8 with the suggested preferred orientation of the individual spins.

butterfly. From the magnetic point of view this structure gives rise to spin frustration effects, which make the prediction of the ground state spin arrangement difficult.

The temperature dependence of χT clearly indicates a ferromagnetic behavior with a ground $S = 10$ state,[156] confirmed by high-field magnetization measurements. At the simplest possible approach, this ground state can be justified by putting six $S = \frac{5}{2}$ spins up and two down. The fit of the temperature dependence of the susceptibility suggested the spin arrangement shown by the arrows in Figure 31, which was experimentally confirmed by a polarized neutron-diffraction experiment (Figure 32).[157] The fit of the suscepti-
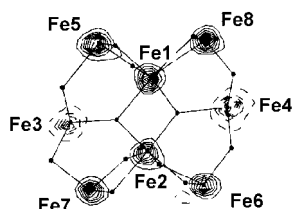

Figure 32. Spin density map of Fe8 from polarized neutron experiments. Negative contours are dashed (step 0.7 μ_B/Å^2). Modified from ref. [157].

bility was performed by assuming a D_2 symmetry for the cluster, which reduced the size of the matrices to be diagonalized.[158] The values of the J constants[83] compare well with the values previously reported for simple iron(III) low-nuclearity compounds with similar bridges.[159] Similar sets of values were also obtained through full-matrix calculations.[83]

The ground $S = 10$ state is largely split in zero-field as shown by HF-EPR,[153,158] inelastic neutron scattering,[160,161] and far infrared spectroscopy.[162] The temperature dependence of the far infrared spectra is shown in Figure 33. Four clear transitions are observed with maxima at 2.45, 2.93, 3.36,
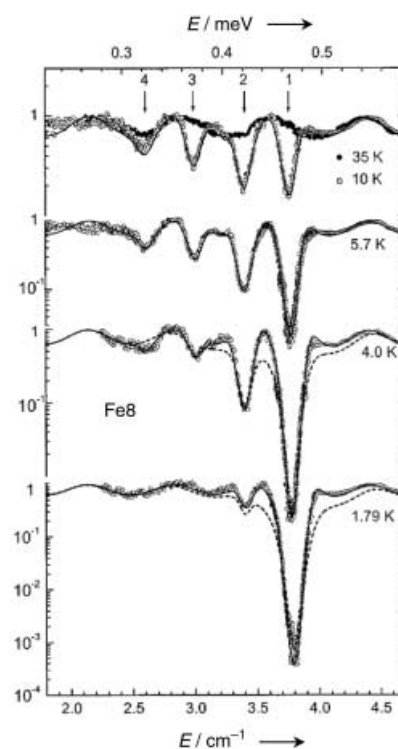

Figure 33. Far infrared spectra of Fe8 in zero field at different temperatures. Modified from ref. [162].

and 3.8 cm^{-1} and are attributed to the transitions $\pm 7 \rightarrow \pm 6$, $\pm 7 \rightarrow \pm 8$, $\pm 8 \rightarrow \pm 9$, and $\pm 9 \rightarrow \pm 10$. Since the cluster has no symmetry the spin Hamiltonian is more complex than that used for Mn12ac. A possible form assuming D_2 symmetry is given by Equation (29), where the O_n^m operators are defined in the Appendix.

$$\mathcal{H} = \mathbf{D}\, S_z^2 + E\,(S_x^2 - S_y^2) + B_4^0 O_4^0 + B_4^2 O_4^2 + B_4^4 O_4^4 \qquad (29)$$

The values of the relevant parameters obtained by the fitting of several different experimental techniques are shown in Table 5. Single-crystal HF-EPR spectra have also provided

Table 5: Zero-field splitting parameters for Fe8.[a]

D	|E/D|	B_4^0	B_4^2	B_4^4	Lit.
−0.205	0.19	1.6×10^{-6}	-5.0×10^{-6}	-8×10^{-6}	[158]
−0.203	0.160	0.7×10^{-6}	8.06×10^{-8}	5.96×10^{-6}	[160]
−0.205	0.150	1.4×10^{-6}	8.06×10^{-8}	5.96×10^{-6}	[162]

[a] See Equation (29).

the directions of the principal axes of the **D** tensor. The easy axis (that of the prevailing orientation of the individual spins) makes a small angle, about 10°, with the perpendicular to the plane of the iron ions, while the hard axis passes through the Fe1 and Fe2 ions. These results show that the splitting has a large rhombic component, mainly determined by the large value of the $|E/D|$ ratio. Consequently the energies of the M_S levels in Fe8 are much different from those of Mn12ac (Figure 34). The lowest-lying levels are almost degenerate $\pm M_S$ pairs, but approaching the top of the barrier the levels are
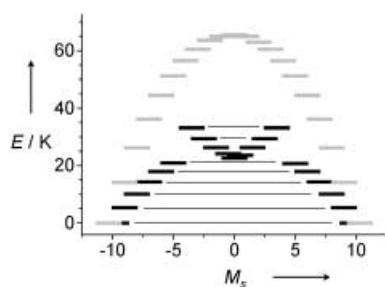
Figure 34. Calculated energy levels of the split components of the $S=$ 10 ground multiplet of Mn12ac (gray) and Fe8 (black). The levels of Fe8 in the upper part of the graph are strongly admixed and their position is arbitrary.

Figure 35. Temperature dependence of the relaxation time of the magnetization of Fe8 (●) and of Fe8PCl (■). Modified from ref. [178].

strongly admixed, and the M_S labeling loses any physical significance. In fact, above the levels which can be indicated as $+5$ and -5 there is a nondegenerate level, which is an admixture of states with smaller M_S. Above this again pairs of quasidegenerate levels are observed, but which cannot be labeled $\pm M_S$. It is apparent that the energy of the barrier in this case cannot be estimated as the difference in energy between the lowest and the highest energy levels. It is probably more appropriate to use the difference between the lowest lying ± 10 and the nondegenerate level. At any rate, there must be a sizeable barrier, therefore slow relaxation effects of the magnetization should be observed at low temperature.

The origin of the magnetic anisotropy responsible for the observed zero-field splitting is presumably a mixture of dipolar and single ion contributions. The dipolar contributions can be easily and rather accurately calculated assuming that the magnetic moments are localized on the iron ions and using the point dipolar approximation.[33] In this frame the calculated zero-field-splitting parameters D and E are much smaller than the experimental values. This is not an unexpected result, because similar trends were observed in other polynuclear iron(III) compounds.[163] Therefore the single ion contribution is also relevant.

Slow relaxation effects show up below 20 K in Mössbauer spectra.[153,154] This technique has a time scale of 10^{-8}–10^{-9} s therefore the blocking temperatures are comparatively higher than in ac susceptibility measurements which show slow relaxation effects only below 3 K. Below 1 K the relaxation time becomes so long that direct measurements can be performed by measuring the magnetization as a function of time. The temperature dependence of the relaxation time of the magnetization in the range 0.070–30 K is shown in Figure 35. At high temperature the Arrhenius law is approximately followed, with $\tau_0 = 2 \times 10^{-7}$ s, and $\Delta/k = 23$ K and with decreasing temperature the curve flattens out. Measurements below 400 mK show that the relaxation time becomes temperature independent ($\tau \approx 5 \times 10^5$ s), thus confirming the presence of pure quantum tunneling.[164]

Like Mn12ac, Fe8 gives rise to a stepped hysteresis.[162,165] In agreement with the smaller zero-field splitting of Fe8 the steps are separated by about 0.22 T and equally spaced. Also, in this case, the steps are attributed to thermally activated tunneling of the magnetization. The dynamic nature of the
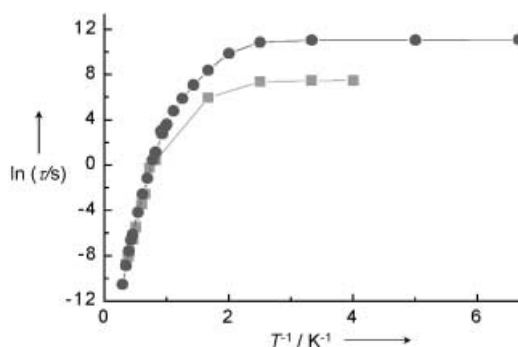
hysteresis is illustrated by the strong dependence of the curves on the sweeping rate of the field (Figure 36).[165,166] The lower the sweep rate the smaller the fraction of molecules that can relax by resonant quantum tunneling at the lower critical fields. Therefore, the steps at higher critical fields increase their height as the sweeping rate is increased. As with the relaxation time the hysteresis becomes temperature independent below 350 mK and this makes Fe8 better suited to investigate all the effects related to the tunneling process. The square-root decay of the magnetization of Equation (23) has been observed in Fe8.[165] The role of the dipolar field and its evolution as the tunneling relaxation proceeds has been monitored with the use of the hole digging micro-SQUID techniques.[127] Under experimental conditions that give the narrowest linewidth for the magnetization hole, the linewidth
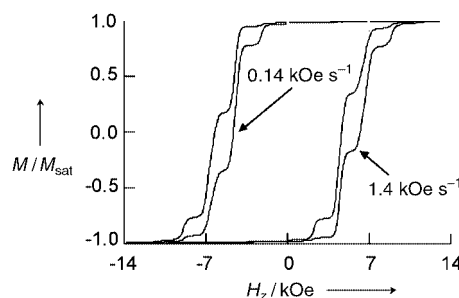

Figure 36. Dependence of the hysteresis loops of Fe8 on the field sweeping rate in the pure tunneling regime ($T = 0.3$ K).

of the hole, about 0.8 mT, is significantly smaller than in Mn12ac, which is in agreement with the reduced hyperfine field of Fe8 in which the only magnetically active iron nucleus is ^{57}Fe, with a natural abundance of about 2%. Nevertheless hyperfine fields play an important role in the tunneling mechanism. In fact for Fe8 the tunnel splitting of the lowest $\pm$ 10 levels corresponds to a field H_t of approximately 10^{-8} T. The dipolar field H_d is of the order of 10–30 mT,[167] thus the tunneling conditions, which require $H_t > H_d$ are not fulfilled. If tunneling is suppressed, the magnetization at very low temperature is frozen and so are the dipolar fields. However the fluctuating hyperfine field H_{hyp}, generated by the magnetic nuclei ^{1}H ($I = ^1/_2$), ^{79,81}Br ($I = ^3/_2$), ^{14}N ($I = 1$) present in the Fe8 clusters, is of the order of 1 mT. The broadening of the ground ± 10 levels may restore the tunneling conditions for

the molecules for which $H_d < H_{hyp}$. Let us suppose that a given molecule undergoes the transition by the tunneling mechanism. Its relaxation changes the dipolar fields of the neighboring molecules in such a way that other molecules reach the tunneling conditions. Therefore the relaxation process is a continuous one.[118,168] The evolution of the magnetization with time as well as the hole digging process have been successfully simulated with Monte Carlo techniques using the tunneling scenario described above.[169,170]

The role of the nuclei in the relaxation process has been demonstrated in experiments in which Fe8 has been enriched with the magnetic ^{57}Fe ($I = \frac{1}{2}$) isotope and/or with ^2H ($I = 1$).[171,172] Enrichment with ^{57}Fe shortens the relaxation time, in agreement with the increased hyperfine field, while the enrichment with deuterium causes an enhancement of the relaxation time, in agreement with the decreased hyperfine field (Figure 37). This unusual isotope effect, which is not related to the mass (which is increased in both isotopically
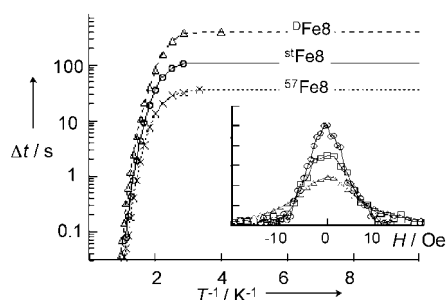

Figure 37. Temperature dependence of the elapsed time needed to relax 1% of the saturation magnetization of a deuterium enriched Fe8 crystal ($^DFe8$), of a standard crystal ($^{st}Fe8$), and of a ^{57}Fe enriched one ($^{57}Fe8$). The inset shows the hole burnt in the distribution of tunneling rate versus applied field for the $^DFe8$ (○), $^{st}Fe8$ (□), and $^{57}Fe8$ (△). Modified from ref. [171].

modified samples), seems to be related to the broadening of the tunneling resonance as confirmed by the investigation of the intrinsic linewidth by the hole-digging technique. The linewidth is larger for the ^{57}Fe enriched sample and smaller for the deuterated one (inset of Figure 37). The observed linewidth for the natural-abundance derivative is in qualitative agreement with the hyperfine fields of the protons determined by NMR spectroscopy.[173,174] The increase in linewidth observed in the enriched sample compares well with an approximation performed taking into account the contact term of the hyperfine interaction of ^{57}Fe nuclei in iron(III) systems.

It is possible to enhance the tunnel splitting by applying a field perpendicular to the easy axis. When the field is applied along the hard direction the oscillating behavior described in Section 5 should than be observed. The measurement of the tunnel splitting can be best performed by using the Landau–Zener–Stückelberg (LZS) model.[175–177] In a two-level system the crossing may occur either directly (zero tunnel splitting) or through an "avoided crossing" (nonzero tunnel splitting; Figure 38). The avoided crossing occurs if the two states are admixed. The admixture can be determined both by intrinsic
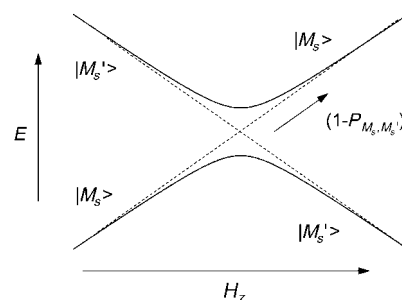

Figure 38. Crossing (– – –) and avoided crossing (——) of pairs of levels as a function of an axial magnetic field.

fields (given by terms such as $E(S_x^2 - S_y^2)$), and by external fields, applied parallel to a hard direction. By sweeping the magnetic field along the easy axis at a relatively high frequency only a small fraction of molecules can tunnel within the short period, thus the dipolar field distribution is not altered. Moreover, if the field is swept over the entire resonance, the dipolar field distribution has no effect on the overall tunnel probability. When sweeping the H_z field at a constant frequency over the avoided energy level in which crossing between the levels M_S and M_S' occurs, the tunneling probability is given by Equation (30) where dH/dt is the constant field sweeping frequency.

$$P_{M_S,M_S'} = 1 - \exp[-\pi\Delta_{M_S,M_S'}^2/(2\,h\,g\mu_B|M_S - M_S'|dH/dt)] \tag{30}$$

If the splitting is zero, P is also zero, and no tunneling occurs. If Δ is large, P tends to one, and tunneling occurs. The magnetization after N sweeps is given by Equation (31) where Γ is the overall LZS transition frequency.

$$M(N) \sim \exp[-2\,P\,N] = \exp[-\Gamma t] \tag{31}$$

Experimentally Γ, P, and Δ can be measured by saturating the magnetization, then periodically changing the field at a constant rate.

Wernsdorfer and Sessoli[51] used the micro-SQUID apparatus described in Section 7.3 and measured the tunnel splitting with the LZS model by sweeping the axial magnetic field around the values of $H_z = n\,0.22$ T, with $n = 0, 1, 2$, which correspond to the tunnel resonance conditions for the $10 \rightarrow -10$, $10 \rightarrow -9$, and $10 \rightarrow -8$ levels, respectively. The measured values of Δ as a function of the applied static transverse field H_x for the quantum transitions between $M_S = +10$ and $M_{S'} = -(10-n)$ are shown in Figure 39. Oscillations with a periodicity of about 0.4 T are clearly seen. These are the first observations of the destructive interference of tunneling pathways (the so-called Berry phase shown in Figure 8) in magnets. The parity effects are clearly seen: the oscillations are symmetric around $H_x = 0$, this corresponds to a maximum value of Δ for $n = 0, 2$, and a minimum for $n = 1$. If the observed values are compared with those which can be calculated using Equations (12) and (13) and the experimentally determined D and E values the agreement is far from satisfactory. An acceptable agreement is only obtained if the fourth-order transverse term is included and a B_4^4 parameter
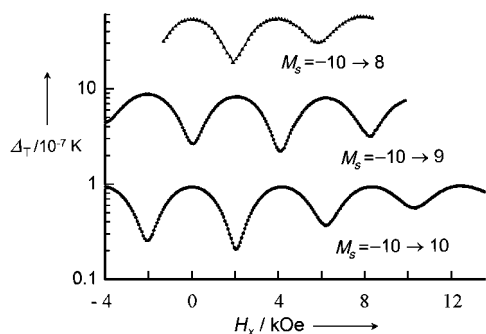
290

Angew. Chem. Int. Ed. **2003**, *42*, 268–297

Figure 39. Transverse-field dependence of the tunnel splitting of quasi-degenerate M,M' levels measured for Fe8 at 80 mK. The three curves corresponds to different resonance fields characterized by $n=0$, $n=1$, and $n=2$. Modified from ref. [51].

about five-times larger than the value provided by HF-EPR.[158] The period of the oscillation, being related to the tunnel splitting of low-lying levels, is however very strongly affected by higher-order terms of the transverse anisotropy, for which no experimental estimates are available. This area requires further theoretical and experimental work.

A transverse field modulation can effect the shape of the hysteresis loop, promoting or suppressing tunneling as shown in Figure 40, where three hysteresis loops measured for Fe8 in
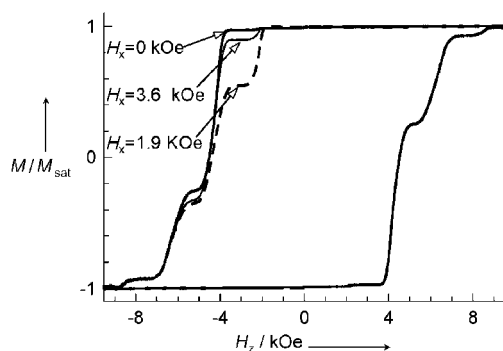

Figure 40. Transverse-field dependence of the hysteresis loop of Fe8 in the ground-state tunneling regime. Modified from ref. [235].

the quantum regime are reported. The three curves differ for the applied transverse static field. A transverse field of 0.19 T significantly enhances the quantum relaxation at the resonance field $H_z = 0.22$ T. The height of the step is larger than both in zero and in a stronger transverse field of $H_x = 0.38$ T. This anomalous behavior is only observed in SMMs, where the tunneling dominates the magnetization dynamics. In principle with the bidimensional control of the field it should be possible to influence the hard–soft magnetic character of the material, as the application of an appropriate transverse field facilitates the reversal of the longitudinal magnetization, without affecting the stability of the remnant magnetization in zero field.

Fe8 is less amenable than Mn12 clusters to ligand substitution reactions. Actually only one other derivative

has been reported, $[Fe_8O_2(OH)_{12}(tacn)_6]Br_{4.3}(ClO_4)_{3.7} \cdot 6 H_2O$ (Fe8PCl), in which some of the bromide ions have been replaced by perchlorate ions.[178] While Fe8 crystallizes in the triclinic space group $P1$,[152] Fe8PCl crystallizes in the monoclinic $P2_1/c$. This change of space group has consequences for the relative orientations of the molecules in the unit cell. In fact two magnetically nonequivalent sites are observed in Fe8PCl which is centrosymmetric. The magnetic properties of the two compounds are very similar to each other. The HF-EPR spectra also show a very similar splitting of the ground $S = 10$ state, with the distinct difference that the second-order transverse anisotropy is larger in Fe8PCl. ($|E/D| = 0.21$ in Fe8PCl and 0.19 for Fe8). This result has consequences for the relaxation times (see Figure 35). The relaxation times of Fe8PCl are shorter because of the larger transverse field anisotropy. The crossover from mixed thermal–quantum to quantum relaxation occurs in both cases at about 350 mK.

9. Other Single-Molecule Magnets

As expected, other clusters have been reported to have SMMs behavior, these include Fe4,[179] Mn4,[180–186] V4,[187] CrM6,[188–191] Ni12,[112] and Mn10.[193] It is apparent that for SMM behavior it is not the size of the clusters that counts but rather the value of S in the ground state and the magnetic anisotropy. However, all these molecules show slow relaxation effects at lower temperatures than Mn12ac.

$[Fe_4(OCH_3)_6(dpm)_6]$ (Fe4; Hdpm = dipivaloylmethane) has the structure shown in Figure 41.[179] The cluster Fe4 crystallizes in the monoclinic space group $C2/c$, with crystallo-
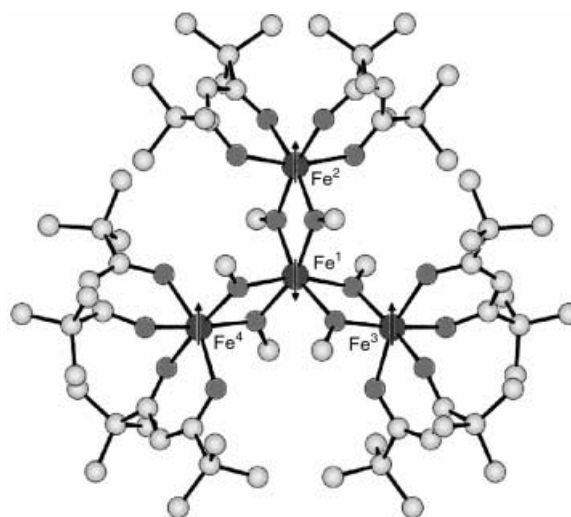

Figure 41. Structure of Fe4 with the suggested preferred orientation of the spins. Fe dark gray, C light gray, O medium gray.

graphically imposed C_2 symmetry, however, there is some disorder, resulting from the dpm units. The four iron(III) ions are antiferromagnetically coupled to give a ground $S = 5$ state, as confirmed by the temperature dependence of the magnetic

susceptibility. Polycrystalline powder HF-EPR spectra give $D = -0.20$ cm^{-1}, which suggests a barrier for the reorientation of the magnetization of about 7 K. More accurate single-crystal investigations performed at W band frequency (95 GHz) showed the presence of three different sites, in agreement with the disordered structure, with slightly different zero-field-splitting parameters.[194] Similar results were obtained by inelastic neutron scattering experiments.[195] The spin dynamics have been studied by Mössbauer spectroscopy, which reveals slow relaxation below 30 K.[154, 196] Slow magnetic relaxation was observed below 1 K ($\tau_0 = 1.1 \times 10^{-6}$ s, $\Delta/k = 3.5$ K), in reasonable agreement with the above zero-field-splitting parameters.

There are now several families of Mn$_4$ clusters which show SMM behavior. The first comprises a central cubane-type structure [Mn$_4$(μ_3-O)$_3$(μ_3-X)]$^{6+}$ (X = Cl, F, N$_3$, NCO, O$_2$CMe), for which a [Mn^{IV}Mn$_3^{III}$] charge distribution is suggested along with a $S = \frac{9}{2}$ ground state, with a large zero-field splitting. The D values obtained from measurements on the temperature dependence of the magnetic susceptibility of polycrystalline powders are in the range -0.27 to -0.32 cm^{-1}. Values of about -0.54 cm^{-1} were estimated from the analysis of HF-EPR spectra.[180] Below 3 K the system shows an out of phase ac susceptibility in zero field and an Arrhenius behavior of the relaxation time. Below 1 K hysteresis loops are observed with well-defined steps at $H = \pm 0.5$ T, which are in agreement with the D value estimated from HF-EPR data. More surprising is the well-defined step observed in zero field, although a half-integer spin should not show tunneling in zero field.[180] In fact, the relaxation becomes temperature independent, suggesting the presence of tunneling.

More recently, another $S = \frac{9}{2}$ cluster, [Mn$_4$O$_3$(OSiMe$_3$)(O$_2$CMe)$_3$(dbm)$_3$] (Hdbm = dibenzoylmethane) has been extensively investigated at low temperature along with a Mn$_2^{II}$Mn$_2^{III}$, $S = 8$, cluster of formula [Mn$_4$(O$_2$CMe)$_2$(Hpdm)$_6$](ClO$_4$)$_2$ (H$_2$pdm = pyridine-2,6-dimethanol). Thanks to the micro-SQUID techniques and the Landau–Zener model the tunnel splitting of the ground state has been investigated as a function of the magnetic field applied perpendicularly to the easy axis.[197] The tunnel splitting increases much faster with increasing transverse field for the $S = \frac{9}{2}$ cluster than the $S = 8$ cluster or the Fe8 cluster which also has an integer spin state. These findings confirm that the tunneling is partially quenched in zero field for half-integer spin. The parity effect in the tunnel splitting is clearly in agreement with Kramers theorem,[34, 56] and the results reported by Wernsdorfer et al.[197] are a nice experimental confirmation of it. In the compound of formula [Mn$_4$O$_3$Cl$_4$(O$_2$CEt)$_3$(py)$_3$] (py = pyridine) two Mn4 clusters, each one characterized by a $S = \frac{9}{2}$ ground state, are connected through weak hydrogen bonds. The effects of this intercluster interaction are also visible in the tunneling of the magnetization, which is suppressed in zero field because at this field both clusters should tunnel at the same time.[198]

Another well documented type of small SMM is provided by compounds of formula [V$_4^{III}$O$_2$(O$_2$CR)$_7$(bpy)$_2$]$^+$ (byp = bipyridine) with a V$_4$O$_2$ core arranged in a butterfly structure.[187] Vanadium(III) is a d^2 ion which in O_h symmetry has an orbitally degenerate ^{3}T$_{1g}$ state. However, neglecting compli-

cations associated with orbital degeneracy the temperature dependence of the magnetic susceptibility suggested a ground $S = 3$ state, with $D = -1.5$ cm^{-1}. This result suggests an energy barrier of about 18 K, but only a very weak out-of-phase signal was observed in the ac susceptibility measurements. Similar parameters were reported for [NEt$_4$]-[V$_4^{III}$O$_2$(O$_2$CR)$_7$(pic)$_2$] (pic = 2-picolinate) in which stronger out-of-phase signals were observed which shift on applying external magnetic fields.

The list of systems showing SMM behavior is continually increasing. Increasing the spin ground state is still the goal of the synthetic efforts of many groups. Spin states larger than ten have in fact been observed in Mn10,[199] Fe19,[200, 201] and Ni12[192, 200, 201] clusters, as well as in heterometallic clusters containing cyanide bridges.[188–190] Despite of the larger spin of the ground state, the magnetic anisotropy is relatively small for these compounds and the blocking temperature is around or below 1 K. Evidence of the thermal-assisted tunneling of the magnetization are often limited to the observation of an Arrhenius behavior with a significantly reduced barrier height, and comparison of the magnetic anisotropy estimated from EPR and magnetic data. A larger database of well-characterized systems could help in clarifying some points, such as the role played by the excited spin states or that played by the anisotropic terms of the intracluster exchange interaction for the still relatively rare phenomenon of resonant magnetic tunneling.

10. Conclusions and Perspectives

The field of single-molecule magnets is still rapidly expanding, and there is no doubt that in the next few years there will be many more compounds available, perhaps with higher blocking temperatures and better controlled quantum effects. Further attempts will also be made to organize the SMMs into layers in which it will be possible to address individual molecules.[202–205]

Other categories of classical molecular magnetic clusters are also being studied. These include the antiferromagnetic rings, which have been suggested to give rise to tunneling effects of the Neél vector,[206, 207] and individual clusters with antiferromagnetic coupling, such as V15[208–211] and Fe30.[212]

Antiferromagnetic rings of different size, but so far only even membered, have been reported. This is a pity because in odd membered rings spin frustration effects might be observed, giving rise to a rich spin dynamics. Interesting quantum effects have been observed in antiferromagnetic rings, of the type [Fe$_{10}$(OMe)$_2$(CH$_2$ClCOO)$_{10}$] (Fe10), the so-called ferric wheel.[213] Below 1 K, Fe10 is in the ground $S = 0$ state, so that the low-field magnetization is zero. However, on increasing the field the excited states with $S > 0$ rapidly decrease their energies, and a crossover between the ground states $S = 0$ and $S = 1$ is observed as a step in the magnetization curve. At higher fields analogous crossovers occur, for example between $S = 2$ and $S = 1$ and, in strong pulsed fields, it was possible to observe the crossover to an $S = 9$ ground state. The position of the steps provides information on the energy separation of the excited states in zero field, assuming

292

Angew. Chem. Int. Ed. **2003**, *42*, 268–297

that the *g* values are known, a reasonable assumption for iron(III) compounds. The stepped magnetization indicates the appearance of the quantum size effects in molecular clusters on a macroscopic scale. However, if the same measurements are performed on $[Mo_{72}Fe_{30}O_{252}\{Mo_2O_7(H_2O)\}_2\{Mo_2O_8H_2(H_2O)\}(CH_3COO)_{12}(H_2O)_{91}]\cdot 150\,H_2O$ (Fe30), completely different results are observed.[212] The molybdenum ions are diamagnetic, therefore the magnetic properties are associated with the 30 iron(III) ions which are located on the vertices of an icosidodecahedron. Because of the geometry of the spin sites and the antiferromagnetic exchange, spin frustration and competing ordered states are expected to occur. The temperature dependence of the magnetic susceptibility gave (using classical spins) $J \approx 1.6\,K$, and the field dependence of the magnetization did not show any quantum size effect down to 0.46 K. The linear increase in magnetization for Fe30 is characteristic of an antiferromagnet. This situation suggests that for Fe30 the spin levels define a quasicontinuum and quantum effects are only expected to show up below 100 mK. In this sense Fe30 can be considered as a tiny antiferromagnet, exactly as Mn12ac can be considered as a tiny ferrimagnet.

In addition to Fe10 there are several other iron(III) antiferromagnetic rings reported (Fe6,[214–220] Fe8,[221] Fe12,[222] Fe18[223]) and also rings comprising different metal ions, such as the chromic wheels.[224–227] Several features of these antiferromagnetic rings are as yet not completely understood. There is clear indication of avoided crossing between the levels, a requisite for observing quantum tunneling in the Landau–Zener approach. Odd spin terms would be required to allow the admixture of neighboring states (with *S* differing by ± 1, as observed at the $S = 0 \rightarrow 1$, $S = 1 \rightarrow 2$, crossovers). The role of Dzyaloshinski–Moriya terms, that is antisymmetric exchange, has been advocated, but this demands non-centrosymmetric structures, however most of the wheels are centrosymmetric.[225,228]

A somewhat similar situation has been observed recently in $K_6[V_{15}As_6O_{42}(H_2O)]\cdot 8\,H_2O$ (V15; $S = 1/2$). This is a cluster comprising fifteen vanadium(IV) ions, with a structure made up of three metal-ion layers containing six, three, and six vanadium ions, respectively.[229] The coupling between the ions in the two hexagonal V_6 layers is strongly antiferromagnetic, in such a way that these layers are in the ground $S = 0$ state at low temperature. The three spins in the triangular V_3 layer are frustrated, with a pair of degenerate spin doublets lying lowest.[208] A "butterfly" hysteresis loop was observed below 200 mK suggesting avoided crossing between the low-lying levels.[209,210] Again the role of the antisymmetric exchange terms is assumed to be important, but more experimental and theoretical work is needed to understand fully the physical properties of V15.

Of course, one of the goals is that of synthesizing larger clusters, because it would be important to obtain systems containing hundreds of magnetic atoms, systems with a size in the mesoscopic regime. The seminal results reported by Müller and co-workers[212,230–234] suggest that this route may be possible. Clearly it is not only necessary to synthesize large molecules, which contain a large number of magnetic centers; it is also necessary to promote suitable magnetic interactions between them. The role of the bridging ligands is thus of paramount importance. So far μ_2, μ_3, and even μ_6 bridging O^{2-}, OR^- groups have been found to be very versatile for promoting strong coupling between transition-metal ions. Another interesting bridging ligand is the CN^- ion, which has also the advantage of being asymmetrical thus inducing selectivity when bridging different transition-metal ions. Other ligands will certainly be investigated in the next years. Particularly promising are sulfur-based ligands, which have the advantage of forming stronger covalent bonds than oxygen, and as a consequence a stronger magnetic interaction. The use of paramagnetic bridging ligands, such as nitronyl nitroxides and semiquinones, may also be anticipated.

The physical conditions for obtaining SMM behavior are understood, an easy axis (Ising) type magnetic anisotropy is required. The physical conditions for achieving this are, for ions such as iron(III), chromium(III), manganese(III), cobalt(II) which have been intensively investigated in the last few years, increasingly clear. We remind that the sources of anisotropy are twofold, either associated with the "building blocks" (single-ion anisotropy) or to the "mortar" connecting them (spin–spin anisotropy). Since the anisotropy is a tensorial property it is determined by the tensorial sum of the local anisotropies.[235] In other words it is not sufficient (and may not even be necessary), to choose individual building blocks with the correct Ising type anisotropy, because the bulk anisotropy of the cluster will actually depend on the geometry of the whole structure. To build-up magnetic anisotropy from the anisotropy of the building blocks, it is certainly a good guideline to exploit transition-metal ions which have orbitally nondegenerate ground states. However it must be remembered that the actual anisotropy of the magnetic molecules depends on how the individual building blocks are spatially oriented one relative to the other. And frankly speaking this still seems to be beyond our control, suggesting that serendipity must play an important role in the development of SMMs.[212,230–235]

If the goal of making SMMs is that of increasing the blocking temperatures, then increasing the number of coupled spins and keeping the interactions between the individual spins as strong as possible is certainly the best way forward. In this sense the ferrimagnetic approach, that is, assembling either different antiferromagnetically coupled spins, or different numbers of antiferromagnetically coupled spins, is the easiest approach. Strong ferromagnetic coupling is rather difficult to develop.

Possible applications of magnetic clusters range from novel magnetic storage media to quantum computing. The possibility of storing information in the nanometer-size magnetic iron(III) core of Ferritin is currently being investigated[236–239] thus it is possible that other similar clusters might well be suitable. In general it may be expected that all the uses of magnetic particles might be extended to molecular clusters, for example, magnetic drug delivery, contrast agents for magnetic resonance imaging (MRI), and magnetocaloric effects. The use of smaller particles has been suggested for implementing Grover's algorithm for quantum computing.[18,239]

Angew. Chem. Int. Ed. **2003**, *42*, 268–297

293

11. Appendix

$$M(N) \sim \exp[-2\,P\,N] = \exp[-\Gamma t] \tag{31}$$

$$O_4^2 = \{[7S_z^2 - S(S+1) - 5](S_+^2 + S_-^2) + (S_+^2 + S_-^2)[7S_z^4 - S(S+1) - 5]\}/4 \tag{A2}$$

$$O_4^4 = (S_+^4 + S_-^4)/2 \tag{A3}$$

$$O_4^3 = [S_z(S_+^3 + S_-^3) + (S_+^3 + S_-^3)S_z]/4 \tag{A4}$$

[1] J.-M. Lehn, *Supramolecular Chemistry. Concepts and Perspectives*, VCH, Weinheim, **1995**.

[2] S. Miyata, H. S. Nalwa, *Organic Electroluminescent Materials and Devices*, Gordon and Breach, Amsterdam, **1997**.

[3] C. Bosshard, R. Spreiter, U. Meier, I. Liakatas, M. Bösch, M. Jäger, S. Manetta, S. Follonier, P. Günter in *Crystal Engineering: From Molecules and Crystals to Materials, Vol. C538*, (Eds.: D. Braga, F. Grepioni, A. G. Orpen), Kluwer, Dordrecht, **1999**, p. 261.

[4] J. J. Girerd, M. Verdaguer, O. Eisenstein, *New J. Chem.* **2000**, *24*, 77.

[5] O. Kahn, *Molecular Magnetism*, VCH, Weinheim, **1993**.

[6] *Magnetism: Molecules to Materials. Molecule Based Materials, Vol. 2* (Eds.: J. S. Miller, M. Drillon), Wiley-VCH, Weinheim, **2001**.

[7] *Magnetism: Molecules to Materials. Nanosized Magnetic Materials, Vol. 3* (Eds.: J. S. Miller, M. Drillon), Wiley-VCH, Weinheim, **2002**.

[8] *Magnetism: Molecules to Materials: Models and Experiments, Vol. 1* (Eds.: J. S. Miller, M. Drillon), Wiley-VCH, Weinheim, **2001**.

[9] For a general review of the different classes of molecular magnetic materials see: *MRS Bull.* **2000**, *25*(11), special issue "molecule-based magnets".

[10] D. Gatteschi, A. Caneschi, L. Pardi, R. Sessoli, *Science* **1994**, *265*, 1054.

[11] G. Christou, D. Gatteschi, D. N. Hendrickson, R. Sessoli, *MRS Bull.* **2000**, *25*, 66.

[12] B. Barbara, L. Gunther, *Phys. World* **1999**, *12*(3) 35.

[13] P. C. E. Stamp, *Nature* **1996**, *383*, 125.

[14] E. M. Chudnovsky, *Science* **1996**, *274*, 838.

[15] A. J. Leggett in *Quantum Tunneling of Magnetization-QTM'94* (Eds.: L. Gunther, B. Barbara), Kluwer, Dordrecht, **1995**, p. 1.

[16] J. A. Jones, *Science* **1998**, *280*, 229.

[17] Y. Makhlin, G. Schon, A. Shnirman, *Nature* **1999**, *398*, 305.

[18] M. N. Leuenberger, D. Loss, *Nature* **2001**, *410*, 789.

[19] A. Caneschi, D. Gatteschi, R. Sessoli, A.-L. Barra, L. C. Brunel, M. Guillot, *J. Am. Chem. Soc.* **1991**, *113*, 5873.

[20] R. Sessoli, D. Gatteschi, A. Caneschi, M. A. Novak, *Nature* **1993**, *365*, 141.

[21] T. Lis, *Acta Crystallogr. Sect. B* **1980**, *36*, 2042.

[22] G. Aromi, S. M. J. Aubin, M. A. Bolcar, G. Christou, H. J. Eppley, K. Folting, D. N. Hendrickson, J. C. Huffman, R. C. Squire, H. L. Tsai, S. Wang, M. W. Wemple, *Polyhedron* **1998**, *17*, 3005.

[23] In a crystal the intermolecular dipolar interactions are expected to lead to magnetic order: X. Martinez-Hidalgo, E. M. Chudnovsky, A. A. Aharony, *Europhys. Lett.* **2001**, *55*, 273; J. F. Fernandez, J. J. Alonso, *Phys. Rev. B* **2000**, *62*, 53. However, if the transition temperature is very low the magnetization freezes without achieving the ordered state.

[24] D. Ringe, G. A. Petsko, *Nature* **1999**, *399*, 417.

[25] D. F. Brougham, R. Caciuffo, A. J. Horsewill, *Nature* **1999**, *397*, 241.

[26] J. Villain, A. Fort, *Eur. Phys. J.* **2000**, *17*, 69.

[27] A. H. Morrish, *The Physical Principles of Magnetism*, Wiley, New York, **1966**.

[28] A. Abragam, B. Bleaney, *Electron Paramagnetic Resonance of Transition Ions*, Dover, New York, **1986**.

[29] J. Villain, F. Hartman-Boutron, R. Sessoli, A. Rettori, *Europhys. Lett.* **1994**, *27*, 159.

[30] *Quantum Tunneling of Magnetization–QTM'94* (Eds.: L. Gunther, B. Barbara), Kluwer, Dordrecht, **1995**.

[31] E. M. Chudnovsky, J. Tejada, *Macroscopic Quantum Tunneling of the Magnetic Moments*, Cambridge University Press, Cambridge, **1998**.

[32] P. C. P. Stamp, E. M. Chudnovsky, B. Barbara, *Int. J. Mod. Phys. B* **1992**, *6*, 1355.

[33] A. Bencini, D. Gatteschi, *EPR of Exchange Coupled Systems*, Springer, Berlin, **1990**.

[34] H. A. Kramers, *Proc. R. Acad. Sci. Amsterdam* **1930**, *33*, 959.

[35] A. Fort, A. Rettori, J. Villain, D. Gatteschi, R. Sessoli, *Phys. Rev. Lett.* **1998**, *80*, 612.

[36] D. A. Garanin, E. M. Chudnovsky, *Phys. Rev. B* **1997**, *56*, 11102.

[37] M. N. Leuenberger, D. Loss, *Europhys. Lett.* **1999**, *46*, 692.

[38] M. N. Leuenberger, D. Loss, *Phys. Rev. B* **2000**, *61*, 1286.

[39] F. Luis, J. Bartolomé, J. F. Fernàndez, *Phys. Rev. B* **1998**, *57*, 505.

[40] T. Pohjola, H. Schoeller, *Phys. Rev. B* **2000**, *62*, 15026.

[41] J. R. Friedman, *Phys. Rev. B* **1998**, *57*, 10291.

[42] F. Hartmann-Boutron, P. Politi, J. Villain, *Int. J. Mod. Phys. B* **1996**, *10*, 2577.

[43] M. N. Leuenberger, D. Loss, *Phys. Rev. B* **2000**, *61*, 12200.

[44] In the treatment in ref. [43] it has been assumed that *S* is a good quantum number, but in light of experimental data this may break down.

[45] A. Garg, *Europhys. Lett.* **1993**, *22*, 205.

[46] D. Loss, D. P. Di Vincenzo, G. Grinstein, *Phys. Rev. Lett.* **1992**, *69*, 3236.

[47] J. von Delft, C. Henley, *Phys. Rev. Lett.* **1992**, *69*, 3236.

[48] A. Garg, *Phys. Rev. B* **2001**, *64*, 4413.

[49] A. Garg, *Phys. Rev. B* **2001**, *64*, 4414.

[50] M. N. Leuenberger, D. Loss, *Phys. Rev. B* **2001**, *63*, 4414.

[51] W. Wernsdorfer, R. Sessoli, *Science* **1999**, *284*, 133.

[52] R. Schilling in *Quantum Tunneling of Magnetization–QTM'94* (Eds.: L. Gunther, B. Barbara), Kluwer, Dordrecht, **1995**, p. 59.

[53] S.-Y. Lee, S.-K. Yoo, *Phys. Rev. B* **2000**, *62*, 13884.

[54] M. V. Berry, *Proc. R. Soc. London Ser. A* **1984**, *392*, 45.

[55] G. Wentzel, *Z. Phys.* **1926**, *38*, 518.

[56] H. A. Kramers, *Z. Phys.* **1926**, *39*, 826.

[57] L. Brillouin, *J. Phys. (Paris)* **1926**, *7*, 353.

[58] J. L. Van Hemmen, A. Sütö in *Quantum Tunneling of the Magnetization–QTM'94* (Eds.: L. Gunther, B. Barbara), Kluwer, Dordrecht, **1995**, p. 19.

[59] A. Garg, *Phys. Rev. Lett.* **1999**, *83*, 4385.

[60] R. F. Weinland, G. Fischer, *Z. Anorg. Allg. Chem.* **1921**, *120*, 161.

[61] M. B. Robin, P. Day, *Adv. Inorg. Chem. Radiochem.* **1967**, *10*, 247.

[62] I. D. Brown, K. K. Wu, *Acta Crystallogr. Sect. B* **1976**, *32*, 1957.

[63] P. Langan, R. Robinson, P. J. Brown, D. Argyriou, D. Hendrickson, G. Christou, *Acta Crystallogr. Sect. C* **2001**, *57*, 909.

[64] A. Cornia, A. C. Fabretti, D. Gatteschi, R. Sessoli, L. Sorace, A. L. Barra, C. Daiguebonne, T. Roisnel, *Acta Crystallogr. Sect. C* **2002**, *58*, M371.

[65] R. Sessoli, H. L. Tsai, A. R. Schake, S. Wang, J. B. Vincent, K. Folting, D. Gatteschi, G. Christou, D. N. Hendrickson, *J. Am. Chem. Soc.* **1993**, *115,* 1804.

[66] H. J. Eppley, H.-L. Tsai, N. de Vries, K. Folting, G. Christou, D. N. Hendrickson, *J. Am. Chem. Soc.* **1995**, *117*, 301.

[67] M. A. Novak, R. Sessoli in *Quantum Tunneling of Magnetization–QTM'94* (Eds.: L. Gunther, B. Barbara), Kluwer, Dordrecht, **1995**, p. 171.

[68] A. L. Barra, D. Gatteschi, R. Sessoli, *Phys. Rev. B* **1997**, *56*, 8192.

[69] A. L. Barra, L. C. Brunel, D. Gatteschi, L. Pardi, R. Sessoli, *Acc. Chem. Res.* **1998**, *31*, 460.

[70] A. Cornia, M. Affronte, A. G. M. Jansen, D. Gatteschi, A. Caneschi, R. Sessoli, *Chem. Phys. Lett.* **2000**, *322*, 477.

[71] S. Hill, J. A. A. J. Perenboom, N. S. Dalal, T. Hathaway, T. Stalcup, J. S. Brooks, *Phys. Rev. Lett.* **1998**, *80*, 2453.

[72] "Molecular Magnetism: From Molecular Assemblies to the Devices": H. U. Güdel, *NATO ASI Ser. E* **1996**, *321*, 229.

[73] I. Mirebeau, M. Hennion, H. Casalta, H. Andres, H. U. Güdel, A. V. Irodova, A. Caneschi, *Phys. Rev. Lett.* **1999**, *83*, 628.

[74] Y. C. Zhong, M. P. Sarachik, J. R. Friedman, R. A. Robinson, T. M. Kelley, H. Nakotte, A. C. Christianson, F. Trouw, S. M. J. Aubin, D. N. Hendrickson, *J. Appl. Phys.* **1999**, *85*, 5636.

[75] A. A. Volkov, Yu. G. Goncharov, G. V. Kozlov, A. A. Mukhin, A. M. Prokhorov, *Infrared Phys.* **1985**, *25*, 369.

[76] A. A. Mukhin, V. D. Travkin, A. K. Zvezdin, S. P. Lebedev, A. Caneschi, D. Gatteschi, *Europhys. Lett.* **1998**, *44*, 778.

[77] A. M. Gomes, M. A. Novak, R. Sessoli, A. Caneschi, D. Gatteschi, *Phys. Rev. B* **1998**, *57*, 5021.

[78] R. A. Robinson, P. J. Brown, D. N. Argyriou, D. N. Hendrickson, S. M. J. Aubin, *J. Phys. Condens. Matter* **2000**, *12*, 2805.

[79] M. R. Pederson, D. V. Porezag, J. Kortus, S. N. Khanna, *J. Appl. Phys.* **2000**, *87*, 5487.

[80] M. R. Pederson, S. N. Khanna, *Phys. Rev. B* **1999**, *60*, 9566.

[81] V. V. Platonov, B. Barbara, A. Caneschi, D. A. Clark, C. M. Fowler, D. G. J. D. Gatteschi, I. A. Lubashevsky, A. A. Mukhin, V. I. Plis, A. I. Popov, D. G. Rickel, R. Sessoli, O. M. Tatsenko, A. K. Zvezdin, unpublished results.

[82] I. Tupitsyn, B. Barbara in *Magnetism: Molecules to Materials. Nanosized Magnetic Materials, Vol. 3* (Eds.: J. S. Miller, M. Drillon), Wiley-VCH, Weinheim, **2002**, p. 109.

[83] C. Raghu, I. Rudra, D. Sen, S. Ramasesha, *Phys. Rev. B* **2001**, *64*, 4419.

[84] Z. G. Soos, S. Ramasesha in *Valence Bond Theory and Chemical Structure* (Eds.: D. J. Klein, N. Trinajstic), Elsevier, New York, **1990**, p. 81.

[85] N. Regnault, T. Jolicoeur, D. Gatteschi, R. Sessoli, M. Verdaguer, *Phys. Rev. B* **2002**, *66*, 054409.

[86] J. K. Cullum, R. A. Willoughby, *Lanczos Algorithm for Large Symmetric Eigenvalue Computations*, Birkhauser, Boston, **1985**.

[87] I. Chiorescu, R. Giraud, A. G. M. Jansen, A. Caneschi, B. Barbara, *Phys. Rev. Lett.* **2000**, *85*, 4807.

[88] M. I. Katsnelson, V. V. Dobrovitski, B. N. Harmon, *Phys. Rev. B* **1999**, *59*, 6919.

[89] D. Gatteschi, L. Sorace, *J. Solid State Chem.* **2001**, *159*, 253.

[90] A. L. Barra, D. Gatteschi, R. Sessoli, G. L. Abbati, A. Cornia, A. C. Fabretti, M. G. Uytterhoeven, *Angew. Chem.* **1997**, *109*, 2423; *Angew. Chem. Int. Ed. Engl.* **1997**, *36*, 2329.

[91] A. Bencini, I. Ciofini, M. G. Uytterhoeven, *Inorg. Chim. Acta* **1998**, *274*, 90.

[92] C. E. Schäffer, *Struct. Bonding (Berlin)* **1973**, *12*, 50.

[93] A. Cornia, R. Sessoli, L. Sorace, D. Gatteschi, A. L. Barra, C. Daiguebonne, *Phys. Rev. Lett.* **2002**, *89*, 257201.

[94] L. Thomas, A. Caneschi, B. Barbara, *Phys. Rev. Lett.* **1999**, *83*, 2398.

[95] M. A. Novak, R. Sessoli, A. Caneschi, D. Gatteschi, *J. Magn. Magn. Mater.* **1995**, *146*, 211.

[96] J. R. Friedman, M. P. Sarachik, J. Tejada, R. Ziolo, *Phys. Rev. Lett.* **1996**, *76*, 3830.

[97] L. Thomas, F. Lionti, R. Ballou, D. Gatteschi, R. Sessoli, B. Barbara, *Nature* **1996**, *383*, 145.

[98] J. A. A. J. Perenboom, J. S. Brooks, S. Hill, T. Hathaway, N. S. Dalal, *Phys. B* **1998**, *246*, 294.

[99] J. A. A. J. Perenboom, J. S. Brooks, S. Hill, T. Hathaway, N. S. Dalal, *Phys. Rev. B* **1998**, *58*, 330.

[100] F. Luis, J. M. Hernandez, J. Bartolome, J. Tejada, *Nanotechnology* **1999**, *10*, 86.

[101] F. Luis, J. Bartolome, J. F. Fernandez, J. Tejada, J. M. Hernandez, X. X. Zhang, R. Ziolo, *Phys. Rev. B* **1997**, *55*, 11448.

[102] J. R. Friedman, M. P. Sarachik, J. M. Hernandez, X. X. Zhang, J. Tejada, E. Molins, R. Ziolo, *J. Appl. Phys.* **1997**, *81*, 3978.

[103] J. M. Hernandez, X. X. Zhang, F. Luis, J. Tejada, J. R. Friedman, M. P. Sarachik, R. Ziolo, *Phys. Rev. B* **1997**, *55*, 5858.

[104] F. Luis, F. L. Mettes, J. Tejada, D. Gatteschi, L. J. de Jongh, *Phys. Rev. Lett.* **2000**, *85*, 4377.

[105] F. Fominaya, J. Villain, T. Fournier, P. Gandit, J. Chaussy, A. Fort, A. Caneschi, *Phys. Rev. B* **1999**, *59*, 519.

[106] F. Fominaya, J. Villain, P. Gandit, J. Chaussy, A. Caneschi, *Phys. Rev. Lett.* **1997**, *79*, 1126.

[107] A. Lascialfari, D. Gatteschi, F. Borsa, A. Shastri, Z. H. Jang, P. Carretta, *Phys. Rev. B* **1998**, *57*, 514.

[108] Z. H. Jang, A. Lascialfari, F. Borsa, D. Gatteschi, *Phys. Rev. Lett.* **2000**, *84*, 2977.

[109] B. Barbara, L. Thomas, F. Lionti, A. Sulpice, A. Caneschi, *J. Magn. Magn. Mater.* **1998**, *177*, 1324.

[110] A. D. Kent, Y. C. Zhong, L. Bokacheva, D. Ruiz, D. N. Hendrickson, M. P. Sarachik, *Europhys. Lett.* **2000**, *49*, 521.

[111] L. Bokacheva, A. D. Kent, M. A. Walters, *Phys. Rev. Lett.* **2000**, *85*, 4803.

[112] Y. C. Zhong, M. P. Sarachik, J. Yoo, D. N. Hendrickson, *Phys. Rev. B* **2000**, *62*, R9256.

[113] E. M. Chudnovsky, D. A. Garanin, *Phys. Rev. Lett.* **1997**, *79*, 4469.

[114] K. M. Mertes, Y. Suzuki, M. P. Sarachik, Y. Paltiel, H. Strickman, E. Zeldov, E. Rumberger, D. N. Hendrickson, G. Christou, *Phys. Rev. Lett.* **2001**, *87*, 227205.

[115] E. M. Chudnovsky, D. A. Garanin, *Phys. Rev. Lett.* **2001**, *8718*, 7203.

[116] R. V. Chamberlin, G. Mozurkewich, R. Orbach, *Phys. Rev. Lett.* **1984**, *52*, 867.

[117] D. K. Lottis, R. M. White, E. Dan Dahlberg, *Phys. Rev. Lett.* **1991**, *67*, 362.

[118] N. V. Prokof'ev, P. C. E. Stamp, *Phys. Rev. Lett.* **1998**, *80*, 5794.

[119] N. V. Prokof'ev, P. C. E. Stamp, *J. Low Temp. Phys.* **1996**, *104*, 143.

[120] F. Fominaya, T. Fournier, P. Gandit, J. Chaussy, *Rev. Sci. Instrum.* **1997**, *68*, 4191.

[121] J. F. Fernandez, F. Luis, J. Bartolome, *Phys. Rev. Lett.* **1998**, *80*, 5659.

[122] W. Wernsdorfer, R. Sessoli, D. Gatteschi, *Europhys. Lett.* **1999**, *47*, 254.

[123] W. Wernsdorfer, K. Hasselbach, A. Benoit, B. Barbara, D. Mailly, J. Tuaillon, J. P. Perez, V. Dupuis, J. P. Dupin, G. Giraud, A. Perex, *J. Appl. Phys.* **1995**, *78*, 7192.

[124] M. Evangelisti, J. Bartolomé, *J. Magn. Magn. Mater.* **2000**, *221*, 99.

[125] S. M. J. Aubin, Z. M. Sun, H. J. Eppley, E. M. Rumberger, I. A. Guzei, K. Folting, P. K. Gantzel, A. L. Rheingold, G. Christou, D. N. Hendrickson, *Inorg. Chem.* **2001**, *40*, 2127.

Angew. Chem. Int. Ed. **2003**, *42*, 268–297

295

[126] W. Wernsdorfer, T. Ohm, C. Sangregorio, R. Sessoli, D. Gatteschi, C. Paulsen, *Phys. B* **2000**, *284*, 1229.

[127] W. Wernsdorfer, *Adv. Chem. Phys.* **2001**, *118*, 99.

[128] X. S. Xie, J. K. Trautman, *Annu. Rev. Phys. Chem.* **1998**, *49*, 441.

[129] F. L. Mettes, F. Luis, L. J. de Jongh, *Phys. Rev. B* **2001**, *64*, 174411.

[130] A. Schenck, *Muon Spin Rotation Spectroscopy: Principles and Applications in Solid State Physics*, Hilger, Bristol, **1986**.

[131] D. Gatteschi, P. Carretta, A. Lascialfari, *Phys. B* **2000**, *289*, 94.

[132] T. Goto, T. Kubo, T. Koshiba, Y. Fujii, A. Oyamada, J. Arai, K. Takeda, K. Awaga, *Phys. B* **2000**, *284*, 1227.

[133] Y. Furukawa, K. Watanabe, K. Kumagai, F. Borsa, D. Gatteschi, *Phys. Rev. B* **2001**, *64*, 4401.

[134] Y. Furukawa, K. Watanabe, K. Kumagai, Z. H. Jang, A. Lascialfari, F. Borsa, D. Gatteschi, *Phys. Rev. B* **2000**, *62*, 14246.

[135] D. Arcon, J. Dolinsek, T. Apih, R. Blinc, N. S. Dalal, R. M. Achey, *Phys. Rev. B* **1998**, *58*, R2941.

[136] J. Dolinsek, D. Arcon, R. Blinc, P. Vonlanthen, J. L. Gavilano, H. R. Ott, R. M. Achey, N. S. Dalal, *Europhys. Lett.* **1998**, *42*, 691.

[137] R. M. Achey, P. L. Kuhns, A. P. Reyes, W. G. Moulton, N. S. Dalal, *Phys. Rev. B* **2001**, *64*, 4420.

[138] A. Lascialfari, Z. H. Jang, F. Borsa, P. Carretta, D. Gatteschi, *Phys. Rev. B* **1998**, *81*, 3773.

[139] Z. M. Sun, D. Ruiz, E. Rumberger, C. D. Incarvito, K. Folting, A. L. Rheingold, G. Christou, D. N. Hendrickson, *Inorg. Chem.* **1998**, *37*, 4758.

[140] D. Ruiz, Z. Sun, B. Albela, K. Folting, J. Ribas, G. Christou, D. N. Hendrickson, *Angew. Chem.* **1998**, *110*, 315; *Angew. Chem. Int. Ed.* **1998**, *37*, 300.

[141] P. D. Boyd, Q. Li, V. B. Vincent, K. Folting, H.-R. Chang, W. E. Streib, J. C. Huffman, G. Christou, D. N. Hendrickson, *J. Am. Chem. Soc.* **1988**, *110*, 8537.

[142] K. Takeda, K. Awaga, T. Inabe, *Phys. Rev. B* **1998**, *57*, R11062.

[143] Y.-G. Wei, S.-W. Zhang, M.-C. Shao, Y.-Q. Tang, *Polyhedron* **1997**, *16*, 1471.

[144] J. An, Z.-D. Chen, J. Bian, J.-T. Chen, S.-X. Wang, S. Gao, G.-X. Xu, *Inorg. Chim. Acta* **2000**, *299*, 28.

[145] P. Artus, C. Boskovic, J. Yoo, W. E. Streib, L. C. Brunel, D. N. Hendrickson, G. Christou, *Inorg. Chem.* **2001**, *40*, 4199.

[146] S. M. J. Aubin, Z. Sun, L. Pardi, J. Krzystek, K. Folting, L.-C. Brunel, A. L. Rheingold, G. Christou, D. N. Hendrickson, *Inorg. Chem.* **1999**, *38*, 5329.

[147] K. Takeda, K. Awaga, *Phys. Rev. B* **1997**, *56*, 14560.

[148] T. Kuroda-Sowa, M. Lam, A. L. Rheingold, C. Frommen, W. M. Reiff, M. Nakano, J. Yoo, A. L. Maniero, L. C. Brunel, G. Christou, D. N. Hendrickson, *Inorg. Chem.* **2001**, *40*, 6469.

[149] M. Soler, S. K. Chandra, D. Ruiz, E. R. Davidson, D. N. Hendrickson, G. Christou, *Chem. Commun.* **2000**, 2417.

[150] M. Soler, S. K. Chandra, D. Ruiz, J. C. Huffman, D. N. Hendrickson, G. Christou, *Polyhedron* **2001**, *20*, 1279.

[151] W. Wernsdorfer, M. Soler, G. Christou, D. N. Hendrickson, *J. Appl. Phys.* **2002**, *91*, 7164.

[152] K. Wieghardt, K. Pohl, I. Jibril, G. Huttner, *Angew. Chem.* **1984**, *96*, 63; *Angew. Chem. Int. Ed. Engl.* **1984**, *23*, 77.

[153] A. L. Barra, P. Debrunner, D. Gatteschi, C. E. Schulz, R. Sessoli, *Europhys. Lett.* **1996**, *35*, 133.

[154] L. Cianchi, F. Del Giallo, G. Spina, W. Reiff, A. Caneschi, *Phys. Rev. B* **2002**, *65*, 064415.

[155] J. B. Vincent, C. Christmas, H.-R. Chang, Q. Li, P. D. W. Boyd, J. C. Huffman, D. N. Hendrickson, G. Christou *J. Am. Chem. Soc.* **1989**, *111*, 2086.

[156] C. Delfs, D. Gatteschi, L. Pardi, R. Sessoli, K. Wieghardt, D. Hanke, *Inorg. Chem.* **1993**, *32*, 3099.

[157] Y. Pontillon, A. Caneschi, D. Gatteschi, R. Sessoli, E. Ressouche, J. Schweizer, E. Lelievre-Berna, *J. Am. Chem. Soc.* **1999**, *121*, 5342.

[158] A. L. Barra, D. Gatteschi, R. Sessoli, *Chem. Eur. J.* **2000**, *6*, 1608.

[159] S. M. Gorun, S. J. Lippard, *Inorg. Chem.* **1991**, *30*, 1625.

[160] R. Caciuffo, G. Amoretti, A. Murani, R. Sessoli, A. Caneschi, D. Gatteschi, *Phys. Rev. Lett.* **1998**, *81*, 4744.

[161] G. Amoretti, R. Caciuffo, J. Combet, A. Murani, A. Caneschi, *Phys. Rev. B* **2000**, *62*, 3022.

[162] A. Mukhin, B. Gorshunov, M. Dressel, C. Sangregorio, D. Gatteschi, *Phys. Rev. B* **2001**, *63*, 4411.

[163] G. L. Abbati, L. C. Brunel, H. Casalta, A. Cornia, A. C. Fabretti, D. Gatteschi, A. K. Hassan, A. G. M. Jansen, A. L. Maniero, L. A. Pardi, C. Paulsen, U. Segre, *Chem. Eur. J.* **2001**, *7*, 1796.

[164] C. Sangregorio, T. Ohm, C. Paulsen, R. Sessoli, D. Gatteschi, *Phys. Rev. Lett.* **1997**, *78*, 4645.

[165] W. Wernsdorfer, T. Ohm, C. Sangregorio, R. Sessoli, D. Mailly, C. Paulsen, *Phys. Rev. Lett.* **1999**, *82*, 3903.

[166] W. Wernsdorfer, R. Sessoli, A. Caneschi, D. Gatteschi, A. Cornia, D. Mailly, *J. Appl. Phys.* **2000**, *87*, 5481.

[167] T. Ohm, C. Sangregorio, C. Paulsen, *Eur. Phys. J. B* **1998**, *6*, 195.

[168] N. V. Prokof'ev, P. C. E. Stamp, *Rep. Prog. Phys.* **2000**, *63*, 669.

[169] A. Cuccoli, A. Fort, A. Rettori, E. Adam, J. Villain, *Eur. Phys. J. B* **1999**, *12*, 39.

[170] J. J. Alonso, J. F. Fernandez, *Phys. Rev. Lett.* **2001**, *87*, 7205.

[171] W. Wernsdorfer, A. Caneschi, R. Sessoli, D. Gatteschi, A. Cornia, V. Villar, C. Paulsen, *Phys. Rev. Lett.* **2000**, *84*, 2965.

[172] R. Sessoli, A. Caneschi, D. Gatteschi, L. Sorace, A. Cornia, W. Wernsdorfer, *J. Magn. Magn. Mater.* **2001**, *226*, 1954.

[173] D. Gatteschi, A. Lascialfari, F. Borsa, *J. Magn. Magn. Mater.* **1998**, *185*, 238.

[174] Y. Furukawa, K. Kumagai, A. Lascialfari, S. Aldrovandi, F. Borsa, R. Sessoli, D. Gatteschi, *Phys. Rev. B* **2001**, *6409*, 4439.

[175] L. Landau, *Phys. Z. Sowjetunion* **1932**, *4*, 46.

[176] C. Zener, *Proc. R. Soc. London Ser. A* **1932**, *137*, 696.

[177] E. C. G. Stückelberg, *Helv. Phys. Acta* **1932**, *5*, 369.

[178] A. L. Barra, F. Bencini, A. Caneschi, D. Gatteschi, C. Paulsen, C. Sangregorio, R. Sessoli, L. Sorace, *ChemPhysChem* **2001**, *2*, 523.

[179] A. L. Barra, A. Caneschi, A. Cornia, F. F. De Biani, D. Gatteschi, C. Sangregorio, R. Sessoli, L. Sorace, *J. Am. Chem. Soc.* **1999**, *121*, 5302.

[180] S. M. J. Aubin, N. R. Dilley, L. Pardi, J. Krzystek, M. W. Wemple, L. C. Brunel, M. B. Maple, G. Christou, D. N. Hendrickson, *J. Am. Chem. Soc.* **1998**, *120*, 4991.

[181] E. K. Brechin, J. Yoo, M. Nakano, J. C. Huffman, D. N. Hendrickson, G. Christou, *Chem. Commun.* **1999**, 783.

[182] A. Yamaguchi, H. Ishimoto, K. Awaga, J. S. Yoo, M. Nakano, D. N. Hendrickson, E. K. Brechin, G. Christou, *Phys. B* **2000**, *284*, 1225.

[183] S. Y. Wang, M. S. Wemple, J. Yoo, K. Folting, J. C. Huffman, K. S. Hagen, D. N. Hendrickson, G. Christou, *Inorg. Chem.* **2000**, *39*, 1501.

[184] J. Yoo, E. K. Brechin, A. Yamaguchi, M. Nakano, J. C. Huffman, A. L. Maniero, L. C. Brunel, K. Awaga, H. Ishimoto, G. Christou, D. N. Hendrickson, *Inorg. Chem.* **2000**, *39*, 3615.

[185] N. Aliaga, K. Folting, D. N. Hendrickson, G. Christou, *Polyhedron* **2001**, *20*, 1273.

[186] A. Bhattacharjee, Y. Miyazaki, M. Nakano, J. Yoo, G. Christou, D. N. Hendrickson, M. Sorai, *Polyhedron* **2001**, *20*, 1607.

[187] S. L. Castro, Z. M. Sun, C. M. Grant, J. C. Bollinger, D. N. Hendrickson, G. Christou, *J. Am. Chem. Soc.* **1998**, *120*, 2365.

[188] T. Mallah, C. Auberger, M. Verdaguer, P. Veillet, *J. Chem. Soc. Chem. Commun.* **1995**, 61.

[189] A. Sciuller, T. Mallah, M. Verdaguer, A. Nivorozkhin, J. L. Tholence, P. Veillet, *New J. Chem.* **1996**, *20*, 1.

[190] A. Sciuller, V. Marvaud, J. Vaissermann, I. Rosenman, M. Verdaguer, *Mol. Cryst. Liq. Cryst. Sci. Technol. Sect. A* **1999**, *334*, 1165.

296

Angew. Chem. Int. Ed. **2003**, *42*, 268 – 297

[191] Z. Salman, A. Keren, P. Mendels, A. Scuiller, M. Verdaguer, *Phys. B* **2000**, *289*, 106.

[192] C. Cadiou, M. Murrie, C. Paulsen, V. Villar, W. Wernsdorfer, R. E. P. Winpenny, *Chem. Commun.* **2001**, 2666.

[193] A. L. Barra, A. Caneschi, D. Gatteschi, D. P. Goldberg, R. Sessoli, *J. Solid State Chem.* **1999**, *145*, 484.

[194] A. Bouwen, A. Caneschi, D. Gatteschi, E. Goovaerts, D. Schoemaker, L. Sorace, M. Stefan, *J. Phys. Chem. B* **2001**, *105*, 2658.

[195] G. Amoretti, S. Carretta, R. Caciuffo, H. Casalta, A. Cornia, M. Affronte, D. Gatteschi, *Phys. Rev. B* **2001**, *64*, 4403.

[196] A. Caneschi, L. Cianchi, F. Del Giallo, D. Gatteschi, P. Moretti, F. Pieralli, G. Spina, *J. Phys. Condens. Matter* **1999**, *11*, 3395.

[197] W. Wernsdorfer, S. Bhaduri, C. Boskovic, G. Christou, D. N. Hendrickson, *Phys. Rev. B.* **2002**, *65*, 180403.

[198] W. Wernsdorfer, N. Allaga-Alcalde, D. N. Hendrickson, G. Christou, *Nature* **2002**, *416*, 406.

[199] D. P. Goldberg, A. Caneschi, R. Sessoli, C. D. Delfs, J. S. Lippard, *J. Am. Chem. Soc.* **1995**, *117*, 5789.

[200] A. K. Powell, S. L. Heath, D. Gatteschi, L. Pardi, R. Sessoli, G. Spina, F. Del Giallo, F. Pieralli *J. Am. Chem. Soc.* **1995**, *117*, 2491.

[201] J. C. Goodwin, R. Sessoli, D. Gatteschi, W. Wernsdorfer, A. K. Powell, S. L. Heath, A. L. Barra, *J. Chem. Soc. Dalton Trans.* **2000**, 4702.

[202] M. Clemente-Leon, H. Soyer, E. Coronado, C. Mingotaud, C. J. Gomez-Garcia, P. Delhaes, *Angew. Chem.* **1998**, *110*, 3053; *Angew. Chem. Int. Ed.* **1998**, *37*, 2842.

[203] M. Clemente-Leon, H. Soyer, C. Mingotaud, C. J. Gomez-Garcia, E. Coronado, P. Delhaes, *Synth. Met.* **1999**, *103*, 2263.

[204] M. Clemente-Leon, E. Coronado, P. Delhaes, C. J. Gomez-Garcia, C. Mingotaud, *Adv. Mater.* **2001**, *13*, 574.

[205] E. Coronado, M. Feliz, A. Forment-Aliaga, C. J. Gomez-Garcia, R. Llusar, F. M. Romero, *Inorg. Chem.* **2001**, *40*, 6084.

[206] A. Chiolero, D. Loss, *Phys. Rev. Lett.* **1998**, *80*, 169.

[207] F. Meier, D. Loss, *Phys. Rev. Lett.* **2001**, *86*, 5373.

[208] D. Gatteschi, L. Pardi, A.-L. Barra, A. Müller, J. Döring, *Nature* **1991**, *354*, 463.

[209] I. Chiorescu, W. Wernsdorfer, B. Barbara, A. Müller, H. Bögge, *J. Appl. Phys.* **2000**, *87*, 5496.

[210] I. Chiorescu, W. Wernsdorfer, A. Müller, H. Bögge, B. Barbara, *Phys. Rev. Lett.* **2000**, *84*, 3454.

[211] I. Chiorescu, W. Wernsdorfer, A. Müller, H. Bögge, B. Barbara, *J. Magn. Magn. Mater.* **2000**, *221*, 103.

[212] A. Müller, M. Luban, C. Schröder, R. Modler, P. Kögerler, M. Axenovich, J. Schnack, P. Canfield, S. Bud'ko, N. Harrison, *ChemPhysChem* **2001**, *2*, 517.

[213] K. L. Taft, C. D. Delfs, G. C. Papaefthymiou, S. Foner, D. Gatteschi, S. J. Lippard, *J. Am. Chem. Soc.* **1994**, *116*, 823.

[214] A. Caneschi, A. Cornia, A. C. Fabretti, S. Foner, D. Gatteschi, R. Grandi, L. Schenetti, *Chem. Eur. J.* **1996**, *2*, 2329.

[215] B. Pilawa, R. Desquiotz, M. T. Kelemen, M. Weickenmeier, A. Geisselmann, *J. Magn. Magn. Mater.* **1997**, *177–181*, 748.

[216] O. Waldmann, J. Schülein, P. Müller, I. Bernt, R. W. Saalfrank, H. P. Andres, H. U. Güdel, P. Allenspach, *Inorg. Chem.* **1999**, *38*, 5879.

[217] G. L. Abbati, A. Cornia, A. C. Fabretti, W. Malavasi, L. Schenetti, A. Caneschi, D. Gatteschi, *Inorg. Chem.* **1997**, *36*, 6443.

[218] A. Lascialfari, Z. H. Jang, F. Borsa, D. Gatteschi, A. Cornia, *J. Appl. Phys.* **1998**, *83*, 6946.

[219] A. Caneschi, A. Cornia, S. J. Lippard, *Angew. Chem.* **1995**, *107*, 511; *Angew. Chem. Int. Ed. Engl.* **1995**, *34*, 467.

[220] M. Affronte, J. C. Lasjaunias, A. Cornia, A. Caneschi, *Phys. Rev. B* **1999**, *60*, 1161.

[221] O. Waldmann, R. Koch, S. Scromm, J. Schülein, P. Müller, I. Bernt, R. W. Saalfrank, F. Hampel, E. Balthes, *Inorg. Chem.* **2001**, *40*, 2986.

[222] A. Caneschi, A. Cornia, A. C. Fabretti, D. Gatteschi, *Angew. Chem.* **1999**, *111*, 1372; *Angew. Chem. Int. Ed.* **1999**, *38*, 1295.

[223] S. P. Watton, P. Fuhrmann, L. E. Pence, A. Caneschi, A. Cornia, G. L. Abbati, S. J. Lippard, *Angew. Chem.* **1997**, *109*, 2917; *Angew. Chem. Int. Ed. Engl.* **1997**, *36*, 2774.

[224] M. Eshel, A. Bino, I. Felner, D. C. Johnston, M. Luban, L. L. Miller, *Inorg. Chem.* **2000**, *39*, 1376.

[225] J. Van Slageren, R. Sessoli, D. Gatteschi, A. A. Smith, M. Helliwell, R. E. P. Winpenny, A. Cornia, A. L. Barra, A. G. M. Jansen, E. Rentschler, G. A. Timco, *Chem. Eur. J.* **2002**, *8*, 277.

[226] I. M. Atkinson, C. Benelli, M. Murrie, S. Parson, R. E. P. Winpenny, *Chem. Commun.* **1999**, 285.

[227] E. J. L. McInnes, C. Anson, A. K. Powell, A. J. Thomson, S. Poussereau, R. Sessoli, *Chem. Commun.* **2001**, 89.

[228] M. Affronte, A. Cornia, A. Lascialfari, F. Borsa, D. Gatteschi, J. Hinderer, M. Horvatic, A. G. M. Jansen, M. H. Julien, *Phys. Rev. Lett.* **2002**, *88*, 167201.

[229] A. Müller, J. Döring, *Angew. Chem.* **1988**, *100*, 1790; *Angew. Chem. Int. Ed. Engl.* **1988**, *27*, 1721.

[230] A. Müller, E. Krickemeyer, S. K. Das, P. Kögerler, S. Sarkar, H. Bögge, M. Schmidtmann, S. Sarkar, *Angew. Chem.* **2000**, *112*, 1674; *Angew. Chem. Int. Ed.* **2000**, *39*, 1612.

[231] A. Müller, C. Beugholt, P. Kögerler, H. Bögge, S. Bud'ko, M. Luban, *Inorg. Chem.* **2000**, *39*, 5176.

[232] A. Müller, S. K. Das, P. Kögerler, H. Bögge, M. Schmidtmann, A. X. Trautwein, V. Schünemann, E. Krickemeyer, W. Preetz, *Angew. Chem.* **2000**, *112*, 3556; *Angew. Chem. Int. Ed.* **2000**, *39*, 3414.

[233] A. Müller, C. Beugholt, H. Bögge, M. Schmidtmann, *Inorg. Chem.* **2000**, *39*, 3112.

[234] A. Müller, P. Kögerler, *Coord. Chem. Rev.* **2000**, *199*, 335.

[235] A. Cornia, D. Gatteschi, R. Sessoli, *Coord. Chem. Rev.* **2001**, *219*, 573.

[236] K. K. W. Wong, T. Douglas, S. Gider, D. D. Awschalom, S. Mann, *Chem. Mater.* **1998**, *10*, 279.

[237] J. G. E. Harris, J. E. Grimaldi, D. D. Awschalom, A. Chiolero, D. Loss, *Phys. Rev. B* **1999**, *60*, 3453.

[238] S. Gider, D. D. Awschalom, T. Douglas, S. Mann, M. Chaparala, *Science* **1995**, *268*, 77.

[239] J. Tejada, E. M. Chudnovsky, E. Del Barco, J. M. Hernandez, T. P. Spiller, *Nanotechnology* **2001**, *12*, 181.

[240] B. Barbara, L. Thomas, F. Lionti, I. Chiorescu, A. Sulpice, *J. Magn. Magn. Mater.* **1999**, *200*, 167.

[241] S. M. J. Aubin, Z. M. Sun, I. A. Guzei, A. L. Rheingold, G. Christou, D. N. Hendrickson, *Chem. Commun.* **1997**, 2239.

Angew. Chem. Int. Ed. **2003**, *42*, 268–297

297